TÜRKİYE
FIRAT UNIVERSITY
GRADUATE SCHOOL OF NATURAL AND APPLIED SCIENCES

INVESTIGATION OF PHYSICAL AND CHEMICAL PROPERTIES OF ANTHRA [2, 3-B, 6, 7-B'] DITHIOPHENE ORGANIC MATERIAL

Hazhar HAMAD RASUL

Master's Thesis

Department of Physics

Program: Molecular Physics

JULY 2020

TÜRKİYE
FIRAT UNIVERSITY
GRADUATE SCHOOL OF NATURAL AND APPLIED SCIENCES

Department of Physics

Master's Thesis

INVESTIGATION OF PHYSICAL AND CHEMICAL PROPERTIES OF ANTHRA [2, 3-B; 6, 7-B'] DITHIOPHENE ORGANIC MATERIAL

Author
Hazhar HAMAD RASUL

Supervisor
Prof. Dr. Niyazi BULUT

Co-Supervisor
Assoc. Prof. Dr. Bayram GÜNDÜZ

JULY 2020
ELAZIĞ

TÜRKİYE

FIRAT UNIVERSITY

GRADUATE SCHOOL OF NATURAL AND APPLIED SCIENCES

Department of Physics

Master's Thesis

Title: Investigation Of Physical And Chemical Properties Of Anthra [2, 3-B; 6, 7-B'] Dithiophene Organic Material

Author: Hazhar HAMAD RASUL

First Delivery Date: 17/06/2020

Defense Date: 08/07/2020

THESIS APPROVAL

This thesis, which was prepared according to the thesis writing rules of the Graduate School of Natural and Applied Sciences, Fırat University, was evaluated by the committee members who have signed the following signatures and was unanimously approved after the defense exam made open to the academic audience.

Signature

Danışman: Prof. Dr. Niyazi BULUT
Firat University, Faculty of Science

Second supervisor: Assoc. Prof. Dr. Bayram GÜNDÜZ
Malatya Turgut Özal University, Faculty of Science

President: Prof. Dr. Sinan AKPINAR
Firat University, Faculty of Science

Member: Assoc. Prof. Dr. Ömer KAYĞILI
Firat University, Faculty of Science

Member: Assoc. Prof. Dr. Sultan ERKAN
Cumhurtiyet University, Faculty of Science

This thesis was registered at the meeting of the Board of Directors of the Institute on ..... / ..... / 20 .....

Signature

Prof. Dr. Soner ÖZGEN
director of Graduate School

DECLARATION

I hereby declare that I wrote this Master's Thesis titled "Investigation Of Physical And Chemical Properties Of Anthra [2, 3-B; 6, 7-B'] Dithiophene Organic Material" in consistent with the thesis writing guide of the Graduate School of Natural and Applied Sciences, Firat University. I also declare that all information in it is correct, that I acted according to scientific ethics in producing and presenting the findings, cited all the references I used, express all institutions or organizations or persons who supported the thesis financially. I have never used the data and information I provide here in order to get a degree in any way.

8 July 2020

Hazhar HAMAD RASUL

PREFACE

In this work, first, HOMO and LUMO have utilized for computation the bad-gap energy. The average band-gap energy between the HOMO and LUMO was found to be 2.84 eV by using five basis sets. After that, the FTIR has been elucidated, in addition, to determine the functional group and determined the important region that did not take place absorption, in general, this region that did not occur absorption is around between the 1650 cm-1 and 3200 cm-1, by suing five basis sets. Then, the UV-Vis spectroscopy was elucidated, in addition, to determine the energy band-gap, that the average energy band gap was found to be 2.59 eV, and it was determined the correct transition type, the ADT molecule exhibited the direct allowed transition.

First of all, I would like to say my appreciation to the Almighty Allah, for his support, generosity and help us to complete my research. I really appreciate that both of my supervisor's reviewed my thesis and they corrected some mistakes about information. So, I want to show my thankfulness and highest thankfulness to my first supervisor's Prof. Dr. Niyazi BULUT, and my second supervisor's Assoc. Prof. Dr. Bayram GÜNDÜZ for all the support and patience that helped me to overcome my problems and their leadership on the right path during my work without him, it would unbelievable to me to accomplish this research. Finally, I want to thank my friend M. Hanifi KEBIROGLU's contribution.

Hazhar HAMAD RASUL
Elazığ, 2020

TABLE OF CONTENTS

Page

ABSTRACT

Investigation of Physical and Chemical Properties of Anthra [2, 3-B; 6, 7-B'] Dithiophene Organic Material

Hazhar HAMAD RASUL

Master's Thesis

FIRAT UNİVERSİTY
Graduate School of Natural and Applied Sciences

Department of Physics
July 2020, Page: xii + 061

The anthradithiophene (ADT) derivative has demonstrated to be a number one in the realm of compact molecule semiconductors (MSs) and is used with various molecules for various electronic applications such as organic photovoltaics (OPVs) and organic field-effect transistors (OFETs). In this study, the theoretical molecular structure of ADT molecule was implemented by using the Gaussian 09W software program. For the theoretical computations, the ADT was optimized by HF and DFT with some basis sets and both methods are most important in quantum mechanical (QM). These two theories are utilized in many areas such as chemistry, physics and materials science to investigate the electronic structure of many body system (MBS). The HF theory is utilized the wave function to describe the energy of molecule, but the DFT is utilized the electron density to describe the energy of molecule. But for all computation, DFT was used since HF theory is not suitable for optimizing this ADT molecule. The highest occupied molecular orbital (HOMO) and the lowest unoccupied molecular orbital (LUMO) were utilized for obtaining band-gap energy. In addition, the electronic potential map (EPM) was indicated and illustrated in detail. After that, the FTIR spectroscopy was demonstrated and showed the important part that did not occur absorption. Next, the UV-Vis spectroscopy was illustrated and this was utilized for determining the correct transition type. On the other hand, experimental FTIR and UV-Vis spectroscopy properties of ADT molecule were investigated in detail and experimental electronic, optical and optoelectronic parameters were obtained. The theoretical and experimental results obtained were compared.

Keywords: Anthradithiophene, Band-gap energy, Electrostatic potential map, DFT, HF

ÖZET

Antra [2, 3-B; 6, 7-B '] Ditiyofen Organik Malzemesinin Fiziksel ve Kimyasal Özelliklerinin Araştırılması

Hazhar HAMAD RASUL

Yüksek Lisans Tezi

FIRAT ÜNİVERSİTESİ
Fen Bilimleri Enstitüsü

Fizik Anabilim Dalı
Temmuz 2020, Sayfa: xii + 061

Antraditiyofen (ADT) türevi, kompakt molekül yarıiletkenleri (MS'ler) alanında bir numara olduğunu göstermiştir ve organik fotovoltaikler (OPV'ler) ve organik alan etkili transistörler (OFET'ler) gibi çeşitli elektronik uygulamalar için çeşitli moleküllerle birlikte kullanılmaktadır. Bu çalışmada, ADT molekülünün teorik moleküler yapısı Gaussian 09W yazılım programı kullanılarak sağlanmıştır. Teorik hesaplamalar için, ADT bazı temel kümelerle HF teorisi ve yoğunluk fonksiyonel teorisi (DFT) tarafından optimize edildi ve her iki yöntem de kuantum mekaniği (QM) için en önemli olanlardır. Bu iki teori, birçok vücut sisteminin (MBS) elektronik yapısını araştırmak için kimya, fizik ve malzeme bilimi gibi birçok alanda kullanılmaktadır. HF teorisi molekülün enerjisini tanımlamak için dalga fonksiyonundan faydalanır, fakat DFT molekülün enerjisini tanımlamak için elektron yoğunluğundan yararlanır. Ancak tüm hesaplamalarda, bu ADT molekülünü optimize etmek için HF teorisi uygun olmadığından DFT kullanılmıştır. Bant aralığı enerjisini elde etmek için, en yüksek işgal edilen moleküler orbital (HOMO) ve en düşük işgal edilmemiş moleküler orbital (LUMO) kullanılmıştır. Ayrıca, elektronik potansiyel haritası (EPM) belirtilmiş ve detaylı olarak gösterilmiştir. Bundan sonra, FTIR spektroskopisi gösterildi ve emilim meydana gelmeyen önemli kısmı gözlendi. Daha sonra, UV-Vis spektroskopisi gösterildi ve bu doğru geçiş tipini belirlemek için kullanıldı. Diğer taraftan, ADT molekülünün deneysel FTIR ve UV-Vis spektroskopisi özellikleri, detaylı bir şekilde araştırıldı ve deneysel elektronik, optik ve optoelektronik parametreler elde edildi. Elde edilen teorik ve deneysel sonuçlar karşılaştırıldı. Son olarak, NMR spektroskopisi aydınlatıldı ve hangisinin hidrojen ve karbondan daha fazla baskın olduğunu ve hangi atomların en büyük elektronegatifliğe ve hangi atomun en düşük elektronegatifliğe sahip olduğunu açıklığa kavuşturmak için kullanıldı.

Anahtar Kelimeler: Antraditiyofen, ADT, Bant aralığı enerjisi, Elektrostatik potansiyel haritası, DFT, HF

LIST OF FIGURES

Page

LIST OF TABLES

Page

SYMBOLS AND ABBREVIATIONS

Symbols

$\emptyset$	: The orbital spin
$\hat{H}$	: The Hamiltonian operator
Ψn	: The many-electron wavefunction
En	: The total energy of the system
$\hat{T}$	: The kinetic energy of the system
$\hat{U}$	: The potential energy of the system
fn	: The Fock operator
χn	: The nth spin-orbital
ε_n	: The nth orbital energy
$\tilde{\nu}$	: The wavenumber
$A_{\tilde{\nu}}$	: The absorbance y
$T_{\tilde{\nu}}$	: The transmittance
μ	: The magnetic moment
η	: The gyromagnetic ratio
E_g	: The optical band gap energy

Abbreviations

OFETs	: Organic field-effect transistors
HF	: Hartree-Fock
DFT	: Density functional theory
HOMO	: The highest occupied molecular orbital
LUMO	: The lowest unoccupied molecular orbital
EPM	: Electronic potential map
RHF	: Restricted Hartree-Fock
UHF	: Unrestricted Hartree-Fock
AO	: Atomic orbital
MO	: Molecular orbital
BSs	: Basis Sets
GBSs	: Gaussian basis sets
GTFs	: Gaussian-Type functions
IP	: Ionization potential
DFs	: Diffuse functions
GBFs	: Gaussian basis functions
CCS	: Correlation consistent set
ECP	: Effective core potential
PP	: Pseudopotential
EMR	: Electromagnetic radiation
IR	: Infrared
NMR	: Nuclear magnetic resonance
PES	: Potential Energy Surfaces

LCs	: Linear combinations
UV-Vis	: Ultraviolet-visible
SVBSs	: Split-Valence Basis Sets
PBSs	: Polarization Basis Sets
HK	: Hohenberg and Kohnin
QM	: Quantum mechanical

1. INTRODUCTION

Computers are currently an important part of the science world, particularly when it comes to calculator problems. For problems which unable to solve analytically, computers and numerical methods are of essential importance.

In a world where we are dependent on the properties of matter that help us improve our lifestyle, it is required to study their properties so that we can utilize them in our service. Matters are due to electronic properties. These matters consist of various types of particles, each with mass and size. These materials are represented by clouds of electrons that oscillate around a net of nuclei, where every single particle interacts with each other within some order, and the main characteristic of the material is due to the electronic properties [1].

In the world, many-particles are interacting in the around us. It is objective is to get insight into the molecular processes observed in the experiment as well as in order to predict them. The determination of molecular and atomic properties is of similar significance in the fields of molecular physics and solid-state physics.

Possibly the most significant fundamental concept of the theory of many-particle is grounded in the view that interacting with the system of many-particle able to describe nearly as a system of non-interacting. Since the quantum mechanics developed in the 1920s, then the Schrödinger equation was introduced in 1926. Various approaches to solving the Schrödinger equation received important attention from physicists and chemists worldwide. With the discovery and development of computers, we are now capable of solving the Schrödinger equation for systems one did not estimate possible less than a century ago.

The primary steps to deal with the analytically and complex not easy to get to know many-body. Schrödinger equation (SE) was accomplished by HF, who derived a set of self-consistent, wave-function based equations which allowed an iterative computation of energies and other described parameters [2, 3]. In atomic and nuclei physics as well as theoretical chemistry, the HF method has using intensively till now.

A way to deal with the lower computational cost of molecular computations can be the use of a less complex base variable. Hohenberg and Kohnin [4] provided the foundation for such an approach in 1964 when they proved that the electron density, a variable only depending on 3 spatial variables, in principle contains all information about the ground state properties of a system. This also appears the birth of the DFT that is devoted to the main part of this thesis. Kohn was granted the Nobel Prize in Chemistry in 1998 for his development of the DFT [5-10]. Kohn and Sham (KS) derived a set of self-consistent in 1965, iteratively solvable equations which finally allowed to use the up to that point only theoretical concept of HK also in actual computer simulations [11-15]. Note the fact that the wave function is a much more complex

quantity than the electron density, the computation times of DFT calculations are mainly lower. DFT is currently successfully applied to a broad variety of quantum mechanical problems, for example, the calculating the ground state properties of interacting many-electron systems such as atoms, molecules or solid band structures in physics and binding molecular energies in chemistry [16], also attempts have making to extend it to obtain excited-states. The approximation makes simpler the model of the electronic system and allows DFT to supply an extremely good balance between cost and computational accuracy [17]. On the other hand, DFT is nowadays one of the most dominant computational procedures for molecular electronic structure computations. The fundamental idea behind this method is that, in terms of the electron probability density, the energy can be calculated for every electronic system. Since electrons are very light particles they require to be labeled by a quantum mechanical approach [18, 19]. In order to understand the procedure, basic knowledge of quantum mechanics is required.

This thesis performs computational calculations on both methods DFT and HF theory for different basis sets, with the purpose of providing which methods is much better than others. All atomic computations and simulations were made using the Gaussian program 09w software and all plot graphs were made using the program of Origin Lab Corporation. To implement both methods DFT and HF theory, firstly, we have to optimize the molecule with different basis sets. After that for the same basis set and method FTIR, NMR and UV calculation are being done. Also, experimental FTIR and UV-Vis spectroscopy properties of ADT molecule were investigated in detail and experimental electronic, optical and optoelectronic parameters were obtained. The theoretical and experimental results obtained were compared. The aim to illustrate the chemical and physical properties of ADT material. First, we will present a short review of HF theory and then concentrate on DFT, after that a brief review of spectroscopy.

2. MATERIALS AND METHODS

In this section, a detailed information about using material and methods in this thesis are given in detail as below.

2.1. Hartree Fock (HF) Approximation

The exact solution of the Schrödinger equation cannot be obtained in the many-electron system by using the existing mathematical approach. For solving approximately, the time-independent Schrödinger equation was developed by HF methods. The HF theory is fundamental too much of electronic structure theory. Figure 2.1 shows the RHF theory and UHF theory [20, 21].

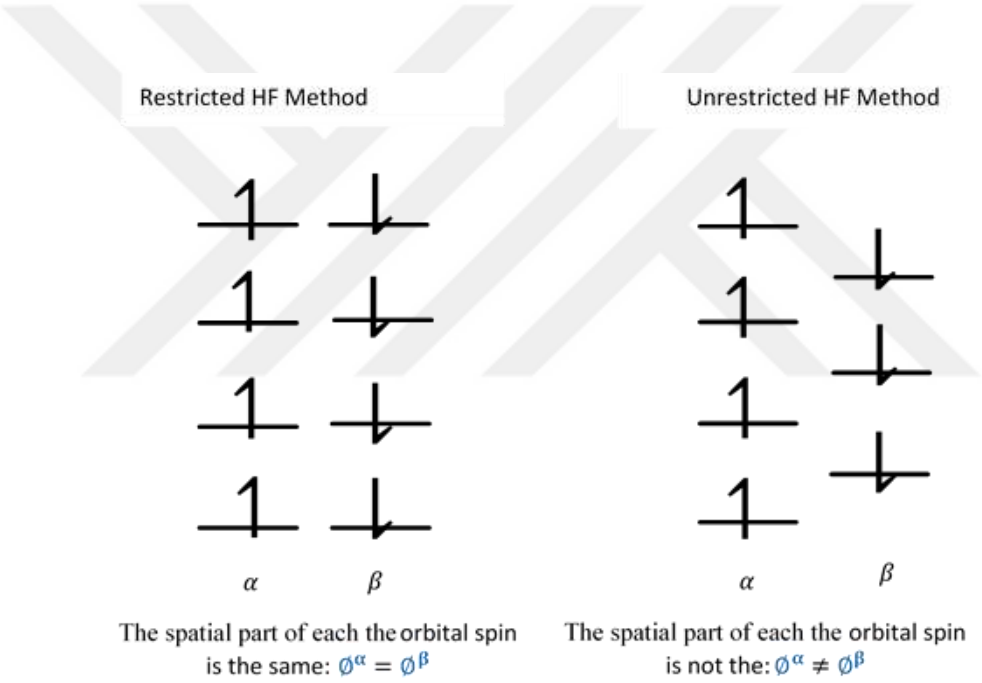

Figure 2.1. Indicate two electrons with opposite spins in RHF method and in UHF [20].

2.1.1. The Schrödinger Equation

In this study, we interested to solve the non-relativist, time-independent, N-electron Schrödinger molecular equation in Quantum Mechanics [22]. First, it is commonly known the single electron Schrödinger equation in atomic units for a single-nucleus atom is

$$(-\frac{1}{2}\nabla^2 + \frac{Z}{r})\,\Psi = E\,\Psi \tag{2.1}$$

The Schrödinger equation tells us everything we can possibly know about a quantum system. We can write the Schrödinger equation for a many-electron system. As shown

$$\hat{H}\,\Psi n = En\,\Psi n \tag{2.2}$$

This is a fundamental quantum mechanics equation. Where $\hat{\mathbf{H}}$, $\boldsymbol{\Psi}_{\mathbf{n}}$, and $\mathbf{E}_{\mathbf{n}}$ are the Hamiltonian operators, the many-electron wavefunction (the different Eigen states) that it describes the state of the system and the corresponding the total energy of the system, respectively. The Hamiltonian operator is given by

$$\hat{H} = \hat{T} + \hat{U} \tag{2.3}$$

$$\hat{H} = \boldsymbol{T}_N + \boldsymbol{T}_e + \boldsymbol{U}_{NN} + \boldsymbol{U}_{N\,e} + \boldsymbol{U}_{e\,e} \tag{2.4}$$

The Hamiltonian Operator of a molecule consisting of **M** nuclei and **N** electrons is expressed as

$$\hat{H}_{mol} = -\sum_{A=1}^{M} \frac{\hbar^2}{2M_A} \nabla_A^2 - \sum_{i=1}^{N} \frac{\hbar^2}{2m_e} \nabla_i^2 + \sum_{A=1}^{M} \sum_{B=A+1}^{M} \frac{Z_A Z_B e^2}{4\pi\varepsilon_o R_{AB}} - \sum_{A=1}^{M} \sum_{i=1}^{N} \frac{Z_A e^2}{4\pi\varepsilon_o r_{i\,A}} + \sum_{i=1}^{N} \sum_{j=i+1}^{N} \frac{e^2}{4\pi\varepsilon_o r_{ij}} \tag{2.5}$$

Which in atomic units (That, "$\mathbf{m_e}$ =1, **e** =1, $\boldsymbol{\hbar}$=1 and $4\boldsymbol{\pi\varepsilon}_o$=1") is given by

$$\hat{H}_{mol} = -\sum_{A=1}^{M} \frac{1}{2M_A} \nabla_A^2 - \sum_{i=1}^{N} \frac{1}{2} \nabla_i^2 + \sum_{A=1}^{M} \sum_{B=A+1}^{M} \frac{Z_A Z_B}{R_{AB}} - \sum_{A=1}^{M} \sum_{i=1}^{N} \frac{Z_A}{r_{i\,A}} + \sum_{i<j}^{N} \frac{1}{r_{ij}} \tag{2.6}$$

Hamiltonian Operator describes all parties included. The many-electron Schrödinger equation cannot be solved exactly (or at least has not been solved) even for a simple two-electron system such as helium atom or hydrogen molecule. Approximations need to be introduced to provide practical methods [23].

2.1.2. The Hartree-Fock Equations

In quantum mechanics, many of the most important problems that we want to solve are all about atoms and molecules. A number of electrons are involved around a number of atomic nuclei. A complete quantum solution of any significant size of such a system is very difficult. HF models are well defined and yield unique properties. There are models of HF applicable to molecules of

more than 50 to 100 atoms [23]. By reducing the total energy of the Schrödinger equation, the n-electron Schrödinger equation (SE) is mathematically transformed to single electron HF equation

$$f_n \chi_n(\boldsymbol{\varkappa}_n) = \varepsilon_n \chi_n(\boldsymbol{\varkappa}_n) \tag{2.7}$$

Where f_n represents the Fock operator; ε_n is an eigenvalue, that represents the energy of orbital. In atom and molecule, AO and MO are given as a solution, respectively. Fock operator is defined as a one-electron operator for an orbital spin:

$$f_n = h_n + \sum_{j\neq n}^{m}\{J_j - K_j\} \tag{2.8}$$

Where h_n represents kinetic energy and Coulomb potential energy between the atomic nucleus and electrons for the nth electron; Kj and Jj are exchange operator and Coulomb operator between the jth and nth electrons, respectively. Note that hi, Jj and Kj are defined as:

$$h_n = -\frac{\hbar^2}{2m_e}\nabla_n^2 - \frac{e^2}{4\pi\varepsilon_0 r_n}\sum_{j=1}^{m} Z_j \tag{2.9}$$

$$J_j\chi_n(\varkappa_n) = \int \chi_j^*(\varkappa_j) r_{nj}^{-1}\, \chi_j(\varkappa_j) d\chi_j \,.\, \chi_n(\varkappa_n) \tag{2.10}$$

$$K_j\chi_n(\varkappa_n) = \int \chi_j^*(\varkappa_j) r_{nj}^{-1}\, \chi_n(\varkappa_j) d\chi_j \,.\, \chi_j(\varkappa_n) \tag{2.11}$$

The nth orbital energy satisfies the following equation.

$$\varepsilon_n = \langle \chi_n(\varkappa_n) | f_n | \chi_n(\varkappa_n) \rangle \tag{2.12}$$

By substituting equations. (2.8), (2.10) and (2.11), Eq. (2.12) is rewritten as:

$$\begin{aligned}\varepsilon_n &= \langle \chi_n(\varkappa_n) | h_n | \chi_n(\varkappa_n) \rangle + \sum_{j\neq 1}^{m} \{\langle \chi_n(\varkappa_n) | J_n | \chi_n(\varkappa_n) \rangle - \langle \chi_n(\varkappa_n) | K_n | \chi_n(\varkappa_n) \rangle\} \\ &= \langle \chi_n(\varkappa_n) | h_n | \chi_n(\varkappa_n) \rangle \\ &+ \sum_{j=1}^{m} \{\langle \chi_n(\varkappa_n)\chi_j(\varkappa_j) | \chi_n(\varkappa_n)\chi_j(\varkappa_j) \rangle - \langle \chi_n(\varkappa_n)\chi_j(\varkappa_j) | \chi_j(\varkappa_n)\chi_n(\varkappa_j) \rangle\}\end{aligned} \tag{2.13}$$

Note that the 2nd and 3rd terms are canceled out when n is equal to j. In the closed-shell system (CSS), the total wave-function of 2n-electron system is showed as

$$\varphi = |\chi_1(\varkappa_1)\,\chi_2(\varkappa_2)\,\cdots\,\chi_{2n-1}(\varkappa_{2n-1})\,\chi_{2n}(\varkappa_{2n})\rangle \tag{2.14}$$

Where χ_n is the nth spin-orbital. As $\boldsymbol{\alpha}$ and β electrons are paired that have the same spatial orbital in the closed-shell system the total wave-function is rewritten as

$$\varphi = |\Psi_1(r_1)\alpha(\omega_1)\Psi_1(r_2)\beta(\omega_2)\cdots\Psi_n(r_{2n})\alpha(\omega_{2n})\Psi_n(r_{2n})\beta(\omega_{2n})\rangle \tag{2.15}$$

The entire energy for the molecule is rewritten as shown below

$$E^{Molecule} = \sum_{n=1}^{m}\langle\chi_n(\varkappa_n)\big|h_n^{Molecule}\big|\chi_n(\varkappa_n)\rangle + \sum_{n=1}^{m}\sum_{j>n}^{m}(J_{nj} - K_{nj}) \tag{2.16}$$

Let us view the entire energy of 2n-electron system. The first term of Equation. (2.16) is rewritten as shown:

$$\begin{aligned}&\sum_{n=1}^{2m}\langle\chi_n(\varkappa_n)|\,h_n|\chi_n(\varkappa_n)\rangle = 2\sum_{n=1}^{m}\langle\chi_n(r_n)\alpha(\omega_n)|h_n|\chi_n(r_n)\alpha(\omega_n)\rangle + \\ &+\sum_{n=1}^{m}\langle\chi_n(r_n)\beta(\omega_n)|h_n|\chi_n(r_n)\beta(\omega_n)\rangle\end{aligned} \tag{2.17}$$

Besides, due to the orthonormality of spin functions, the above equation is rewritten:

$$\sum_{n=1}^{2m}\langle\chi_n(\varkappa_n)|\,h_n|\chi_n(\varkappa_n)\rangle = 2\sum_{n=1}^{m}\langle\chi_n(r_n)|\,h_n|\chi_n(r_n)\rangle \tag{2.18}$$

The 2nd term of Eq. (2.16) is rewritten as shown below

$$\begin{aligned}&\tfrac{1}{2}\sum_{n=1}^{m}\sum_{j=1}^{m}\langle\Psi_n(r_n)\alpha(\omega_n)\Psi_j(r_j)\alpha(\omega_j)\big|\Psi_n(r_n)\alpha(\omega_n)\Psi_j(r_j)\alpha(\omega_j)\rangle\ + \\ &+\tfrac{1}{2}\sum_{n=1}^{m}\sum_{j=1}^{m}\langle\Psi_n(r_n)\alpha(\omega_n)\Psi_j(r_j)\beta(\omega_j)\big|\Psi_n(r_n)\alpha(\omega_n)\Psi_j(r_j)\beta(\omega_j)\rangle \\ &+\tfrac{1}{2}\sum_{n=1}^{m}\sum_{j=1}^{m}\langle\Psi_n(r_n)\beta(\omega_n)\Psi_j(r_j)\alpha(\omega_j)\big|\Psi_n(r_n)\beta(\omega_n)\Psi_j(r_j)\alpha(\omega_j)\rangle \\ &+\tfrac{1}{2}\sum_{n=1}^{m}\sum_{j=1}^{m}\langle\Psi_n(r_n)\beta(\omega_n)\Psi_j(r_j)\beta(\omega_j)\big|\Psi_n(r_n)\beta(\omega_n)\Psi_j(r_j)\beta(\omega_j)\rangle\end{aligned} \tag{2.19}$$

Bye means of the orthonormality of spin functions, the above equation is rewritten as

$$\sum_{n=1}^{m}\sum_{j=1}^{m}2\langle\Psi_n(r_n)\Psi_j(r_j)\big|\Psi_n(r_n)\,\Psi_j(r_j)\rangle = \sum_{n=1}^{m}\sum_{j=1}^{m}2J_{nj} \tag{2.20}$$

The 3rd term of Equation. (2.13) is rewritten as

$$-\frac{1}{2}\sum_{n=1}^{m}\sum_{j=1}^{m}\langle\Psi_n(r_n)\alpha(\omega_n)\Psi_j(r_j)\alpha(\omega_j)|\Psi_n(r_n)\alpha(\omega_n)\Psi_j(r_j)\alpha(\omega_j)\rangle -$$
$$\frac{1}{2}\sum_{n=1}^{m}\sum_{j=1}^{m}\langle\Psi_n(r_n)\alpha(\omega_n)\Psi_j(r_j)\beta(\omega_j)|\Psi_n(r_n)\alpha(\omega_n)\Psi_j(r_j)\beta(\omega_j)\rangle -$$
$$\frac{1}{2}\sum_{n=1}^{m}\sum_{j=1}^{m}\langle\Psi_n(r_n)\beta(\omega_n)\Psi_j(r_j)\alpha(\omega_j)|\Psi_n(r_n)\beta(\omega_n)\Psi_j(r_j)\alpha(\omega_j)\rangle -$$
$$\frac{1}{2}\sum_{n=1}^{m}\sum_{j=1}^{m}\langle\Psi_n(r_n)\beta(\omega_n)\Psi_j(r_j)\beta(\omega_j)|\Psi_n(r_n)\beta(\omega_n)\Psi_j(r_j)\beta(\omega_j)\rangle \quad (2.21)$$

Bye means of the orthogonality of spatial orbitals, the equation (2.21) is rewritten as shown below

$$-\sum_{n=1}^{m}\sum_{j=1}^{m}\langle\Psi_n(r_n)\Psi_j(r_j)|\Psi_n(r_n)\,\Psi_j(r_j)\rangle = -\sum_{n=1}^{m}\sum_{j=1}^{m}K_{nj} \quad (2.22)$$

Finally, the entire energy of the 2n-electron CShS is rewritten as shown:

$$E = 2\sum_{n=1}^{m}\langle\Psi_n(r_n)|h_n|\Psi_n(r_n)\rangle + \sum_{n=1}^{m}\sum_{j=1}^{m}(2J_{nj} - K_{nj}) \quad (2.23)$$

The nth orbital energy is rewritten in the same way:

$$\varepsilon_n = \langle\chi_n(\varkappa_n)|h_n|\chi_n(\varkappa_n)\rangle\sum_{j=1}^{m}(2J_{nj} - K_{nj}) \quad (2.24)$$

In CShS, there is one restriction that $\boldsymbol{\alpha}$-spin and β-spin electrons are paired in the same spatial orbital. HF in the closed-shell system (CSHS) is called restricted RHF. In the open-shell system (OShS), the total wave-function of the n-electron system is expressed as shown

$$\varphi = |\chi_1(\varkappa_1)\,\chi_2(\varkappa_2)\,\chi_3(\varkappa_3)\cdots\,\chi_n(\varkappa_n)\rangle \quad (2.25)$$

Where χ_n is the nth spin-orbital. Notice that spatial orbital is theoretically distinguished by electron spin. The numbers of $\boldsymbol{\alpha}$ and β electrons are indicated as n^{α} and n^{β}, respectively.

$$n = n^{\alpha} + n^{\beta} \quad (2.26)$$

Via utilizing the spatial orbital and spin function, spin orbitals of $\boldsymbol{\alpha}$ spin are showed as

$$\Psi_1^{\alpha}(r_1^{\alpha})\alpha(\omega_1^{\alpha}), \Psi_2^{\alpha}(r_2^{\alpha})\alpha(\omega_2^{\alpha}), \cdots \Psi_{n^{\alpha}}^{\alpha}(r_{n^{\alpha}}^{\alpha})\alpha(\omega_{n^{\alpha}}^{\alpha}) \quad (2.27)$$

In the same way, spin orbitals of β spin are showed as

$$\Psi_1^{\beta}\left(r_1^{\beta}\right)\beta\left(\omega_1^{\beta}\right),\Psi_2^{\alpha}\left(r_2^{\beta}\right)\beta\left(\omega_2^{\beta}\right),\cdots\Psi_{n^{\beta}}^{\beta}\left(r_{n^{\beta}}^{\beta}\right)\beta\left(\omega_{n^{\beta}}^{\beta}\right) \tag{2.28}$$

Notice that position and spin coordinates are separately defined in $\boldsymbol{\alpha}$ and β spins. When n^{β} is smaller than n^{α}, Eq. (2.25) is rewritten as

$$\varphi = |\Psi_1^{\alpha}(r_1^{\alpha})\alpha(\omega_1^{\alpha})\Psi_1^{\beta}(r_1^{\beta})\beta(\omega_1^{\beta})\cdots\Psi_{n^{\alpha}}^{\alpha}(r_{n^{\alpha}}^{\alpha})\rangle \tag{2.29}$$

The 1st term of Eq. (2.16) is rewritten as shown below

$$\begin{aligned}\textstyle\sum_{n=1}^{m}\langle\chi_n(\varkappa_n)|\,h_n|\chi_n(\varkappa_n)\rangle &= \textstyle\sum_{n=1}^{m^{\alpha}}\langle\Psi_n^{\alpha}(r_n^{\alpha})\alpha(\omega_n^{\alpha})|h_n|\Psi_n^{\alpha}(r_n^{\alpha})\alpha(\omega_n^{\alpha})\rangle\\ &+\textstyle\sum_{n=1}^{m^{\beta}}\left\langle\Psi_n^{\beta}(r_n^{\beta})\beta(\omega_n^{\beta})\middle|h_n\middle|\Psi_n^{\beta}(r_n^{\beta})\beta(\omega_n^{\beta})\right\rangle\end{aligned} \tag{2.30}$$

Because of the orthogonality of spin functions, the equation (2.30) is rewritten as

$$\begin{aligned}\textstyle\sum_{n=1}^{m}\langle\chi_n(\varkappa_n)|\,h_n|\chi_n(\varkappa_n)\rangle &= \textstyle\sum_{n=1}^{m^{\alpha}}\langle\Psi_n^{\alpha}(r_n^{\alpha})|h_n|\Psi_n^{\alpha}(r_n^{\alpha})\rangle +\\ \textstyle\sum_{n=1}^{m^{\beta}}\left\langle\Psi_n^{\beta}\left(r_n^{\beta}\right)\middle|h_n\middle|\Psi_n^{\beta}\left(r_n^{\beta}\right)\right\rangle\end{aligned} \tag{2.31}$$

The 2nd term of Equation. (2.16) is rewritten as

$$\begin{aligned}&\tfrac{1}{2}\textstyle\sum_{n=1}^{m^{\alpha}}\sum_{j=1}^{m^{\alpha}}\left\langle\Psi_n^{\alpha}(r_n^{\alpha})\alpha(\omega_n^{\alpha})\Psi_j^{\alpha}(r_j^{\alpha})\alpha(\omega_j^{\alpha})\middle|\Psi_n^{\alpha}(r_n^{\alpha})\alpha(\omega_n^{\alpha})\Psi_j^{\alpha}(r_j^{\alpha})\alpha(\omega_j^{\alpha})\right\rangle\\ &+\tfrac{1}{2}\textstyle\sum_{n=1}^{m^{\alpha}}\sum_{j=1}^{m^{\beta}}\left\langle\Psi_n^{\alpha}(r_n^{\alpha})\alpha(\omega_n^{\alpha})\Psi_j^{\beta}(r_j^{\beta})\beta(\omega_j^{\beta})\middle|\Psi_n^{\alpha}(r_n^{\alpha})\alpha(\omega_n^{\alpha})\Psi_j^{\beta}(r_j^{\beta})\beta(\omega_j^{\beta})\right\rangle\\ &+\tfrac{1}{2}\textstyle\sum_{n=1}^{m^{\beta}}\sum_{j=1}^{m^{\alpha}}\left\langle\Psi_n^{\beta}(r_n^{\beta})\beta(\omega_n^{\beta})\Psi_j^{\alpha}(r_j^{\alpha})\alpha(\omega_j^{\alpha})\middle|\Psi_n^{\beta}(r_n^{\beta})\beta(\omega_n^{\beta})\Psi_j^{\alpha}(r_j^{\alpha})\alpha(\omega_j^{\alpha})\right\rangle\\ &+\tfrac{1}{2}\textstyle\sum_{n=1}^{m^{\beta}}\sum_{j=1}^{m^{\beta}}\left\langle\Psi_n^{\beta}(r_n^{\beta})\beta(\omega_n^{\beta})\Psi_j^{\beta}(r_j^{\beta})\beta(\omega_j^{\beta})\middle|\Psi_n^{\beta}(r_n^{\beta})\beta(\omega_n^{\beta})\Psi_j^{\beta}(r_j^{\beta})\beta(\omega_j^{\beta})\right\rangle\end{aligned} \tag{2.32}$$

By means of the orthogonality of spin functions, the equation (2.32) is rewritten as

$$\begin{aligned}&\tfrac{1}{2}\textstyle\sum_{n=1}^{m^{\alpha}}\sum_{j=1}^{m^{\alpha}}\left\langle\Psi_n^{\alpha}(r_n^{\alpha})\,\Psi_j^{\alpha}\left(r_j^{\alpha}\right)\middle|\Psi_n^{\alpha}(r_n^{\alpha})\Psi_j^{\alpha}\left(r_j^{\alpha}\right)\right\rangle\\ &+\tfrac{1}{2}\textstyle\sum_{n=1}^{m^{\alpha}}\sum_{j=1}^{m^{\beta}}\left\langle\Psi_n^{\alpha}(r_n^{\alpha})\Psi_j^{\beta}\left(r_j^{\beta}\right)\middle|\Psi_n^{\alpha}(r_n^{\alpha})\Psi_j^{\beta}\left(r_j^{\beta}\right)\right\rangle\\ &+\tfrac{1}{2}\textstyle\sum_{n=1}^{m^{\beta}}\sum_{j=1}^{m^{\alpha}}\left\langle\Psi_n^{\beta}\left(r_n^{\beta}\right)\Psi_j^{\alpha}\left(r_j^{\alpha}\right)\middle|\Psi_n^{\beta}\left(r_n^{\beta}\right)\Psi_j^{\alpha}\left(r_j^{\alpha}\right)\right\rangle\\ &+\tfrac{1}{2}\textstyle\sum_{n=1}^{m^{\beta}}\sum_{j=1}^{m^{\beta}}\left\langle\Psi_n^{\beta}\left(r_n^{\beta}\right)\Psi_j^{\beta}\left(r_j^{\beta}\right)\middle|\Psi_n^{\beta}\left(r_n^{\beta}\right)\Psi_j^{\beta}\left(r_j^{\beta}\right)\right\rangle\end{aligned} \tag{2.33}$$

The 3rd term of Eq. (2.16) is rewritten as shown below

$$-\frac{1}{2}\sum_{n=1}^{m^\alpha}\sum_{j=1}^{m^\alpha}\langle\Psi_n^\alpha(r_n^\alpha)\alpha(\omega_n^\alpha)\Psi_j^\alpha(r_j^\alpha)\alpha(\omega_j^\alpha)\left|\Psi_j^\alpha(r_n^\alpha)\alpha(\omega_n^\alpha)\Psi_n^\alpha(r_j^\alpha)\alpha(\omega_j^\alpha)\right\rangle$$
$$-\frac{1}{2}\sum_{n=1}^{m^\alpha}\sum_{j=1}^{m^\beta}\left\langle\Psi_n^\alpha(r_n^\alpha)\alpha(\omega_n^\alpha)\Psi_j^\beta(r_j^\beta)\beta(\omega_j^\beta)\right|\left.\Psi_j^\alpha(r_n^\alpha)\beta(\omega_n^\alpha)\Psi_n^\beta(r_j^\beta)\alpha(\omega_j^\beta)\right\rangle$$
$$-\frac{1}{2}\sum_{n=1}^{m^\beta}\sum_{j=1}^{m^\alpha}\left\langle\Psi_n^\beta(r_n^\beta)\beta(\omega_n^\beta)\Psi_j^\alpha(r_j^\alpha)\alpha(\omega_j^\alpha)\right|\left.\Psi_j^\beta(r_n^\beta)\alpha(\omega_n^\beta)\Psi_n^\alpha(r_j^\alpha)\beta(\omega_j^\alpha)\right\rangle$$
$$-\frac{1}{2}\sum_{n=1}^{m^\beta}\sum_{j=1}^{m^\beta}\left\langle\Psi_n^\beta(r_n^\beta)\beta(\omega_n^\beta)\Psi_j^\beta(r_j^\beta)\beta(\omega_j^\beta)\right|\left.\Psi_j^\beta(r_n^\beta)\beta(\omega_n^\beta)\Psi_n^\beta(r_j^\beta)\beta(\omega_j^\beta)\right\rangle \quad (2.34)$$

Because of the orthogonality of spin functions, the equation (2.34) is rewritten as shown below

$$-\frac{1}{2}\sum_{n=1}^{m^\alpha}\sum_{j=1}^{m^\alpha}\langle\Psi_n^\alpha(r_n^\alpha)\Psi_j^\alpha(r_j^\alpha)\left|\Psi_j^\alpha(r_n^\alpha)\Psi_n^\alpha(r_j^\alpha)\right\rangle$$
$$-\frac{1}{2}\sum_{n=1}^{m^\beta}\sum_{j=1}^{m^\beta}\left\langle\Psi_n^\beta\left(r_n^\beta\right)\Psi_j^\beta\left(r_j^\beta\right)\right|\left.\Psi_j^\beta\left(r_n^\beta\right)\Psi_n^\beta\left(r_j^\beta\right)\right\rangle \quad (2.35)$$

In conclusion, by utilizing notations of Coulomb and exchange integrals, the entire energy of the n-electrons CShS is handed by

$$E=\sum_{n=1}^{n^\alpha}\langle\Psi_n^\alpha(r_n^\alpha)|h_n|\Psi_n^\alpha(r_n^\alpha)\rangle+\sum_{n=1}^{n^\beta}\left\langle\Psi_n^\beta\left(r_n^\beta\right)\right|h_n\left|\Psi_n^\beta\left(r_n^\beta\right)\right\rangle+$$
$$\frac{1}{2}\sum_{n=1}^{m^\alpha}\sum_{j=1}^{m^\alpha}\left(J_{nj}^{\alpha\alpha}-K_{nj}^{\beta\beta}\right)+\frac{1}{2}\sum_{n=1}^{m^\beta}\sum_{j=1}^{m^\beta}\left(J_{nj}^{\beta\beta}-K_{nj}^{\beta\beta}\right)+\frac{1}{2}\sum_{n=1}^{m^\alpha}\sum_{j=1}^{m^\beta}J_{nj}^{\alpha\beta} \quad (2.36)$$

The nth orbital energy of $\boldsymbol{\alpha}$ atomic orbital is reworded in the same style:

$$\varepsilon_n^\alpha=\langle\,\Psi_n^\alpha(r_n^\alpha)|h_n|\,\Psi_n^\alpha(r_n^\alpha)\rangle\sum_{j=1}^{m^\alpha}(J_{nj}^{\alpha\alpha}-\,K_{nj}^{\alpha\alpha})+\sum_{j=1}^{m^\beta}J_{nj}^{\alpha\beta} \quad (2.37)$$

The nth orbital energy of β atomic orbital is reworded in the same way**:**

$$\varepsilon_n^\beta=\left\langle\,\Psi_n^\beta(r_n^\beta)\right|h_n\left|\,\Psi_n^\beta(r_n^\beta)\right\rangle\sum_{j=1}^{m^\beta}(J_{nj}^{\beta\beta}-\,K_{nj}^{\beta\beta})+\sum_{j=1}^{m^\alpha}J_{nj}^{\alpha\beta} \quad (2.38)$$

In OShS, the spatial orbital of $\boldsymbol{\alpha}$ electron is independent from β electron. HF in open-shell system (OSHS) is called UHF [21].

2.1.3. Basis Sets

A set of mathematical functions is a set of basis, linear combinations (LCs) yielding molecular orbitals (MOs). Physically, some basis functions (BFs) prescribe the electron distribution around an atom and joining atomic BFs incomes the electron distribution in the molecular as a whole. BFs not centered on atoms can be considered to lie on atoms. BSs for use in practical HF, density functional computations make use of Gaussian-Type functions. Gaussian functions are approximately related to exponential functions, which are of the form of exact solutions to the one-electron hydrogen atom, and consist of a polynomial in the Cartesian coordinates followed by an exponential in r^2. Some series of Gaussian basis sets (GBSs) now have got popular use and are thoroughly documented. A brief of all-electron basis sets obtainable in Spartan is provided in the Table 2.1 [23]. Except for STO-3G and 3-21G, any of these BSs can be supplemented with additional polarization functions (means adding orbitals with angular momentums) and with diffuse functions. It should be paid attention that minimal (STO-3G) and split-valence (3-21G) basis sets, which deficiency polarization functions, are inappropriate for use with correlated models, in special density functional models [23].

Table 2.1. All-Electron GBSs Obtainable in Spartan.

Basis Sets	**Obtainable elements**
STO-3G	H-Xe
3-21G, 3-21G*	H-Xe
6-31G*, 6-31G** 6-31+G*, 6-31+G** 6-31++G*, 6-31++G**	H-Kr
6-311G*, 6-311G** 6-311+G*, 6-311+G** 6-311++G*, 6-311++G**	H-Ar
cc-pV(D, T, Q)Z	H-Ar, Ga-Kr

Different types of functions have been suggested for contracted GTFs. The following are several important basic functions of the Gaussian type.

- **Minimal Basis Set (MBS) (STO-3G)**

A basis set describes only one BF (STO, GTO, or CGTO) for each atomic orbital in the atom. The most common MBS is STO-nG, where n is an integer [24]. This n value denotes the number of Gaussian primitive (GP) functions involving a single BF. In these basis sets, the same number of GPs comprise core and valence orbitals. Usually, n<3 gives poor result so STO-3G is called the MBS. The simplest possible atomic orbital representation is termed a MBS. This comprises only those functions necessary to accommodate all of the electrons of the atom, while still preserving its

overall spherical symmetry. In practice, this includes a single (1s) function for hydrogen (H) and helium (He), a set of five functions (1s, 2s, 2px, 2py, 2pz) for lithium (Li) to neon (Ne). The STO-3G basis set has two apparent defects: The first defect describing that atom with nearly spherical molecular environments will be better than atoms with a spherical molecular environment. This suggests that evaluations among different molecules will be biased in favor of those incorporating the most spherical atoms. The second defect describing that basis functions are atom centered. This restricts their flexibility to describe electron distributions between nuclei.

- **Split-Valence Basis Sets (SVBSs) (3-21G, 6-31G, and 6-311G)**

The first defect of a MBS may be addressed by providing two sets of valence basis functions inner and outer functions. A split-valence basis set describes only one BF for core atomic orbits and more BFs for valence atomic orbitals. Split-valence was been developed by Pople and coworkers. Hydrogen (H) is provided by two s-type functions, and main-group elements are provided two sets of valence s- and p-type functions. There are (3-21G) and (6-31G) among the simplest SVBSs. Each core atomic orbital in the basis set (3-21G) is expanded in terms of three Gaussians, while BFs representing inner and outer of valence atomic orbitals are expanded to include two and one Gaussian components, respectively. For instance, the BSs (6-31G) represented with reference to six Gaussians and valence orbitals split into three and one Gaussian components. Also, valence-shell can split greater than two. For instance, the basis sets (6-311G) split the valence functions into three parts instead of two parts.

- **Polarization Basis Sets (PBSs) (6-31G*, 6-31G**, 6-311G* and 6-311G**)**

SVBSs could be improved by adding orbitals with different shapes. PBSs add orbitals with angular momentums going beyond of requirement for the proper explanation of the ground state of each atom at the HF level. The second defecting of a MBS, that the atomic orbitals are atom centered, must now be resolved. This could be resolute by adding functions that are off-centered from the nuclei [2]. This is a risky solution, however, because it becomes easy to bias the result. The result is to add p-type functions on H “hydrogen” and d-type functions on main-group heavy atoms that permit the displacement of the electron density away from the nuclear positions [25]. These types of BSs are called PBSs. Examples of PBSs include (6-31G*) and (6-31G**). In a BS of (6-31G*), d-type orbitals are added to heavy main group elements. In a BS of (6-31G**), p-type orbitals are added to hydrogen along with the d-type orbitals in heavy main group elements. Also, polarization functions are functions of a greater angular momentum than the occupied orbitals, such as adding d-orbitals to C “carbon” or f-orbitals to iron (Fe). These orbitals assist the wave function better span the function space. This consequences in little additional energy.

- **Diffuse sets (DSs)**

Diffuse functions (DFs), denoted in Pople-type sets by a plus sign, +, (designated by “+”as in 6-311+G**), it is also possible to add diffuse functions to hydrogens (designated by “++” as in 6-

311++G**) Two plus signs indicate that diffuse functions are also added to light atoms (hydrogen and helium). These are very shallow Gaussian basis functions (GBFs), which more accurately represent the "tail" portion of the AOs, which are distant from the atomic nuclei. These additional BFs can be important when considering anions and other large, "soft" molecular systems. It is common to add additional DFs to a basis [20]. The most frequent reason for doing this is to describe orbitals with a large spatial extent, such as the HOMO of an anion or Rydberg orbitals. Adding DFs can also result in a greater tendency to develop BSSE.

- **Correlation consistent set (CCS)**

Ones of the most broadly used BSs are those developed by Dunning and coworkers. The BSs generally used with correlated models, including density functional models, MP2 models and configuration interaction models, are in fact based on HF calculations [26]. Normally, Gaussian exponents and linear expansion coefficients are first determined to minimize the HF energy of the ground-state atom and are then uniformly scaled to reflect the “tighter” nature of atoms in molecules. Designed to converge systematically to the complete basis set (CBS) limit using extrapolation techniques, for first- and second-row atoms, the BSs are (cc-pVNZ) where cc-p represented the correlation consistent-polarized, the ’V’ indicates they are valence only BSs, D meaning double (Triple, Quadruple) and Z denoted Zeta. They contain consecutively larger shells of polarization functions (d, f, g…etc.).

- **Effective core potential (ECP)**

The function modeling the core electrons is usually called an ECP in the chemical community, while the physics community uses the term PP. Calculations involving heavy elements, in particular, transition metals, can be simplified by explicitly considering only the valence while replacing the core by some form of potential. This includes so-called “pseudopotentials (PP)”. There are four major steps in designing a PP [27].

1) Generate a good-quality all-electron wave function for the atom. This will normally be from a numerical HF, a relativistic DHF or a density functional calculation.
2) Replace the valence orbitals by a group of nodeless pseudo-orbitals. The regular valence orbitals can have radial nodes so as to form them orthogonal to the core orbitals, and also the pseudo-orbitals are designed specified they behave properly within the outer part, however, while not the nodal structure within the core region
3) Replace the core electrons by a potential parameterized by expansion into a suitable set of analytical functions of the distance between nuclear and electron, for instance, a polynomial or a set of Gaussian functions. Since relativistic effects are mainly significant for the core electrons, this potential can effectively contain relativity. The potential may be different for each angular momentum.

4) Fit the parameters of the potential such that the solutions of the Schrödinger equation produce pseudo-orbitals corresponding the all-electron valence orbitals

Molecular systems have traditionally been described by GTBSs. When using Gaussian functions for describing the valence orbitals, it is natural to also use Gaussian functions to describe the ECP. Since Gaussian functions are continuous, there is no fixed distance to characterize the extent of the core potential and the quality of the ECP is determined by the number of electrons chosen to be denoted by the ECP.

2.1.4. The Charge Density

If we have an electron described by the spatial wave function $\boldsymbol{\Psi}_b(r)$, then the probability of finding that electron in a volume element **dr** at a point r is $|\Psi_b(r)|^2$ dr [28]. The probability distribution is $|\Psi_b(r)|^2$. If we have a closed-shell molecule described by a single determinant wave function with each occupied MO $\boldsymbol{\Psi}_b$ containing two electrons, then the total charge density is just

$$\rho(r) = 2\sum_b^{N/2}|\Psi_b(r)|^2 \tag{2.39}$$

Such that $\rho(r)dr$ is the probability of finding any electron in dr at r. The integral of this charge density is just the entire number of electrons,

$$\int dr\rho(r) = 2\sum_b^{N/2}\int dr\,|\Psi_b(r)|^2 = 2\sum_b^{N/2}1 = N \tag{2.40}$$

These equations show that the total charge density for each of the electrons is just a sum of charge densities for a single determinant. We ought to introduce a set of Q known basis functions $\{\boldsymbol{\Phi}n(r) / n = 1, 2, 3 \ldots Q\}$ and expand the unknown molecular orbitals in the linear expansion.

$$\Psi_u = \sum_{n=1}^{Q} C_{nu}\Phi_n \qquad a = 1,2,3,\ldots Q \tag{2.41}$$

When we insert the MO expansion equation (2.40) into the expansion equation (2.38) for the charge density, we can get

$$\rho(r) = 2\sum_b^{N/2}\ \Psi_b^*(r)\Psi_b(r)\ = 2\sum_b^{\frac{N}{2}}\sum_u\ C_{ub}^*\ \Phi_u^*(r)\sum_n C_{nb}\Phi_n(r) =$$

$$\sum_{nu}\left[2\sum_b^{\frac{N}{2}} C_{nb}C_{ub}^*\right]\Phi_n(r)\Phi_u^*(r)$$

$$\rho_{nu} = \sum_{nu}\ P_{nu}\,\Phi_n(r)\Phi_u^*(r) \tag{2.42}$$

Where we have defined a density matrix, so it is sometimes called, a charge density bond order matrix.

$$\mathrm{P_{nu}} = 2\sum_{\mathrm{b}}^{\mathrm{N/2}} \mathrm{C_{nb}C_{ub}^{*}} \tag{2.43}$$

From (2.42), given a set of known basis functions $\{\boldsymbol{\Phi}\mathrm{n}\}$, the matrix P specifies completely the charge density$\rho(r)$ [21]. It is directly related to the expansion coefficients **C** by (2.43), and we can characterize the results of closed-shell HF calculations either by the P_{nu}.

2.1.5. Electron Correlation

The HF method reproduces quantitatively the electronic structure quantitatively. However, the interaction between electron and electron, which is called the effect of electron correlation, is treated theoretically in an average way [21].

Typically, the HF method accounts for about 99.5% percent of the electronic energy, and several chemical properties, and such as polarizabilities, force constants, magnetizabilities, dipole moments and excitation energies, are typically off by less than 10 percent. The problem with HF is that it does not contain all effect of electron correlation. The widest definition of electron correlation is saying that the position of the single electron depends on all other the position of electrons. However, in the mean HF approach field, each electron interacts only through an average potential with the other electrons and fails to account for the instantaneous repulsion effects of electron-electron. Also, it includes the electron correlation enforced by the anti-symmetry of the HF wave function. This correlation is called the Fermi correlation and accounts for most of the correlation. Also note that whenever the HF wave function consists of more than one Slater determinant, this leads to the containing additional electron correlation effects.

In the theory of wave function, the term electron correlation is usually reserved to depict the correlation that occurs upon super-positions of configuration state functions, that is, the difference between the exact consequence and the HF. This leads to the Löwdin definition of the energy of electron correlation, he explains that the energy of correlation for a sure state with reference to an identified Hamiltonian is the variance between the expectation value of the Hamiltonian and its exact eigenvalue in the HF approximation of the state under consideration. The first calculations integrating correlation of electron in helium atom were published by Egil Andersen. Also, the first correlation of electron calculations for molecules was applied by Fritz Wolfgang London and Walter Heitler [26].

2.2. Density Functional Theory (DFT)

The DFT is a phenomenally successful approach to finding solutions to the basic equation for atom and molecular the quantum behavior, the Schrodinger equation (SE) in settings of practical value. The DFT approach is the most broadly used method in quantum chemistry. The basis for DFT is the proof by Hohenberg and Kohn [4] that the ground state electronic energy is determined wholly by the density of electron, In other words, there exists a 1 to -1 correspondence between the electron density of the energy and a system [6, 11].

2.2.1. Basic Theory

The principle behind DFT is that in place of a wave function, the energy of a molecule can determine from the electron density. This theory initiated with a Hoenburg and Kohn theorem (HKT) that stated this was probable. The fundamental theorem applied merely to discover the state of ground electronic energy of a molecule. Kohn and Sham (KS) developed a practical application of this theory, formulating a manner similar to the HF method in the structure [22].

Electron density is expressed in this formulation as a linear combination (LC) of basis functions alike in mathematical form. A determinant is then formed from these functions is called orbitals of KS. It is the density of electron that is utilized to compute the energy from this determinant of orbitals. This process is needed since Fermion systems can only have a density of electrons that arise from an antisymmetric wave function. There has been some discussion over the description of the orbitals of KS. They are certainly not mathematically equivalent from correlated calculations to either natural orbitals or HF orbitals [29]. KS orbitals, withal, to describe the behavior of electrons in a molecule, as do other orbitals mentioned. The orbital eigenvalues of DFT do not counterpart the energies obtained from photoelectron spectroscopy experiments as do HF orbital energies. The questions still under discussion are how similarities can be assigned and how differences can be physically interpreted.

A functional density is then used to achieve the density of electron density energy. In this case, a functional is a function of the density of electron. The exact functional density is mysterious. For that reason, there is a complete list of various functionals that may have advantages or disadvantages [30]. Some of these functionals have advanced by parameterizing functions and some have been from fundamental quantum mechanics to best reproduce experimental results. Consequently, there are in core semiempirical and ab initio versions of DFT. tends to be classified on its own as either an ab initio method or in a class [31].

The advantage of to use the density of electron is that the integrals for Coulomb repulsion necessity be done merely over the density of electron, which is a three-dimensional function, thus scaling as

N^3. In addition, it is possible to include at least several electron correlations in the calculation. This consequences in faster calculations than HF calculations (that scale as N^4) and calculations that are a bit more precise as well.

Finally, indicate the entire field of DFT rests on two fundamental mathematical theorems proven by Kohn and Hohenberg, and the derivation of a set of equations by KS [32]. First, there exists a 1-to-1 mapping between the ground state wave function and the ground state density of electron. Second, the density of electron that minimizes the energy of the above functional is the true density of electron corresponding to the full solution to the Schrodinger equation.

2.2.2. Band Gap

The energy difference between the top of the highest filled band and the bottom of the lowest empty band are called the band-gap. In molecular systems, the top of the highest filled band is corresponding to Highest Occupied Molecular Orbital (HOMO) and the bottom of the lowest empty band is corresponding to the Lowest Unoccupied Molecular Orbital (LUMO), it is called virtual orbitals. When electrons want to jump from one band to another band, it requires a specific minimum amount of energy is called the energy band-gap. Schematic drawing of the relationship between the HOMO–LUMO energy gap in the Figure 2.2. To determine the energy gap some researchers use molecule computations to estimate it [27].

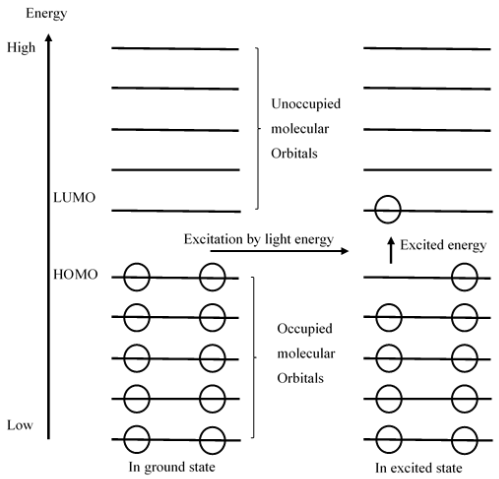

Figure. 2.2. Schematic drawing of the relationship between the HOMO–LUMO energy gap [27].

2.3. Spectroscopy

Spectroscopy is commonly dealing with the absorption and emission of electromagnetic radiation by atoms and molecules, which may be in the gas, liquid, or solid phase [33]. Visible electromagnetic radiation is called light, although the terms light, radiation, and electromagnetic radiation (EMR) can be used interchangeably. Spectroscopy plays a key role in the development of quantum mechanics (QM) and it is essential to understanding molecular properties since the quantum mechanical description of molecular properties [34]. It also is a technique used to determine the structure of a compound by the study of the interaction between matter and EMR such as Infrared (IR), Ultraviolet-visible (UV-Vis) and Nuclear magnetic resonance (NMR) spectroscopy. To find out the interaction between mater and EMR, it is significant to understand the properties of the molecule and that will give us information about the structure and physical properties of the molecule. In this section, we touch on brief information about IR, UV-Vis and NMR spectroscopy.

2.3.1. IR Spectroscopy

IR spectroscopy is a significant analytical technique for determining the structure of a compound (both inorganic and organic compounds) [35]. IR radiations refer broadly to that part of EM spectrum between microwave regions and visible in dictated in the Table 2.2. It means the IR region has lower energy than visible radiation and higher energy than a microwave. IR radiations lie in the wavelength range of (0.75 - 400) μm.

Table 2.2. Indicated the range of the IR spectrum

Region	**Wavelength (nm)**	**Wave number (cm^{-1})**	**Frequency (GHz)**
Near-IR (NIR)	750 – 2500	13333 - 4000	400000 - 120000
Mid-IR (MIR)	2500 – 20000	4000 - 500	120000 - 15000
Far-IR (FIR)	20000 – 400000	500 - 25	15000 - 750

When a molecule absorbs radiation with a frequency of less than 100 cm^{-1} molecular rotation takes place and if a molecule absorbs more than 100 cm^{-1} molecular vibrations occur. Note a single vibrational energy change is accompanied by a large number of rotational energy changes. Three main processes through which a molecule can absorb radiation involves an increase of energy which is proportional to the light absorbed.

First way take place when absorption of radiation leads to a higher rotational energy level in a rotational transition. Second, take place when absorption of radiation leads to a higher vibrational

energy level in a vibrational transition. Indicated the Energy level diagram for a molecule in the Figure 2.3. Third, take place when absorption of radiation leads to a higher electronic energy level in its electronic transitions.

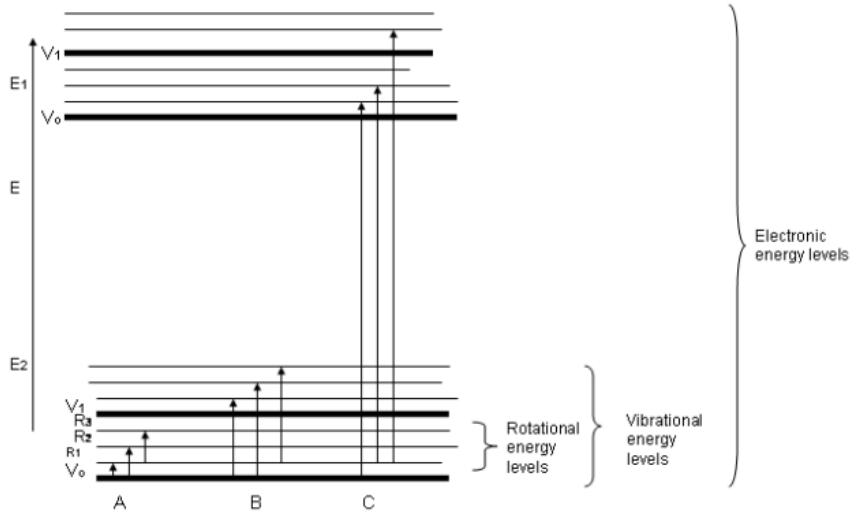

Figure 2.3. Indicated the Energy level diagram for a molecule [35].

2.3.2. UV-VIS Spectroscopy

One of the oldest ways of molecular spectroscopy is UV-Vis spectroscopy. UV-Vis spectroscopy is one of the most common investigative techniques since it is very useful and able to detect closely every molecule. UV-Vis can be used in a qualitative method to recognize functional groups or by matching the absorbance spectrum to confirm the identity of a compound [34]. Usually, UV-Vis is not the utmost sensitive spectroscopy technique, since not much light is absorbed over a short path length and has a similar sensitivity to other measurements of absorbance, such as IR spectroscopy.

The optical spectroscopy is based on the frequency relationship between Bohr and Einstein

$$\Delta E=E_2-E_1= h\nu \tag{2.44}$$

This relationship associates the discrete atomic or molecular energy states En with the frequency v of the electromagnetic radiation (EMR). Where the constant Plank "h=6.626 x 10^{-34} j.s". In spectroscopy, wavenumber $\tilde{\nu}$ should be used instead of frequency v. Since $\nu=c/\lambda=c\tilde{\nu}$, from Eq. 2.45 obtains.

$$\Delta E=E_2-E_1=hc\tilde{\nu} \quad (2.45)$$

Where c is the speed of light, specific energy differences can be assigned to absorbed or emitted radiation of wave number $\tilde{\nu}$. In 1852, Bouguer-Lambert-Beer provided the law systems the mathematical-physical foundation of light absorption measurements on the gases and clarifications in the UV-Vis and IR area.

$$\log\left(\frac{I_o}{I}\right)_{\tilde{\nu}} = \log\left(\frac{100}{T\%}\right)_{\tilde{\nu}} = A_{\tilde{\nu}}$$
$$A_{\tilde{\nu}} = \varepsilon_{\tilde{\nu}}.c.L \quad (2.46)$$

Where $A_{\tilde{\nu}}$ is the absorbance, $T_{\tilde{\nu}} = (I/I_o)*100$ in % is the transmittance and $\varepsilon_{\tilde{\nu}}$ is the molar decadic extinction coefficient. Also, I am the intensity of this emerging from the sample, I_o is the intensity of the monochromatic light entering the sample, c is the concentration of the light-absorbing the substance and L is the path length of the sample in cm. The appearance of wide bands or shoulders on the UV - Vis structure is due to a molecule's numerous vibrational and rotational states, resulting in separate energy band gaps of slightly different energies. It is shown in Figure 2.4.

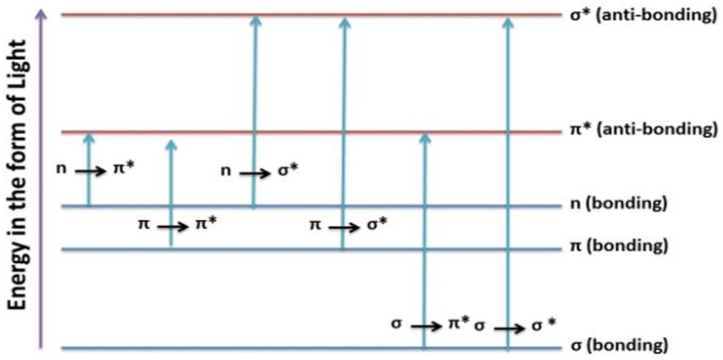

Figure 2.4. This diagram showing their relative energies [36].

The most common transitions falling within the range of UV-Vis are n- π* and π-π*. π orbitals arise caused by double bonds and n orbitals are used by non-bonding electrons. π* are anti-bonding π orbitals. The best absorption of UV-Vis is provided by double bond molecules. Π orbitals adjacent to each other that are linked is called conjugation, usually increases absorption. Sigma star (σ*) transitions, associated with single bonds, are higher energy and fall into the deep UV, also they are fewer useful for routine use.

2.3.3. NMR Spectroscopy

At Stanford and M.I.T, firstly, in 1946 the research groups developed NMR spectroscopy in the USA. The radar technology was developed during the second world war, also it was made several of the electronics aspects of the NMR spectroscopy possible [36]. The chemists and physicists began to apply the anew developed hardware to problems of the chemistry and physics. NMR developed over the next fifty years into the leading organic spectroscopy obtainable to chemists to investigate the giving of information about the chemical structure of they were producing such as chemicals [37].

The phenomenon of NMR is built on the structure atomic nuclei that have properties of magnetic which can be used to get information about the chemical [38]. The subatomic particles of quantum mechanics (QM) are such as neutron, proton, and electron that they have spin [39]. These atoms that their atomic number has paired the nucleus has no spin such as (^{A}X, Where X is element and A= 2, 4, 6 …). Nevertheless, these atoms that their atomic number that denoted by A is unpaired the nucleus does possess spin such as (^{A}X, A= 1, 3, 5 …). To investigate the result of spin can use the following rules:

First, if each number of protons (Z) and neutrons (N) are even, it means the nucleus has no spin. Second, if the sum of the number of Z and N is odd, it means the nucleus has a half-integer spin (1/2, 3/2…etc.). Third, if the sum of the number of Z and N is even, it means the nucleus has an integer spin (1, 2 ... etc.). Splitting of the energy levels for an I=1/2, under an applied magnetic field in the Figure 2.5. In QM terms, the nuclear magnetic moment of a nucleus will align with an outside applied a magnetic field in only 2I+1 way.

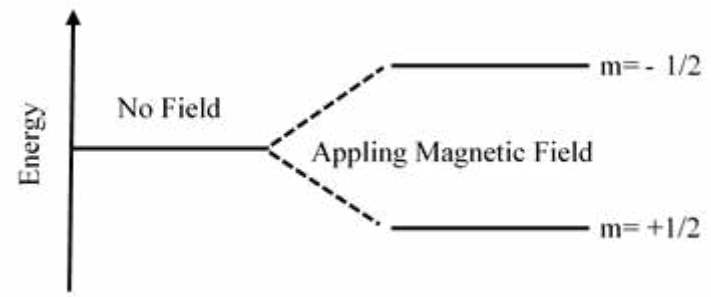

Figure 2.5. Splitting of the energy levels for an I=1/2, under an applied magnetic field [38].

Basic information of NMR, contain an intrinsic property such as electrons and called as spin [38]. The spin of a nucleus can describe using quantum mechanics (QMs). All molecules with a non-zero spin have a magnetic moment is denoted by μ, are given by

$$\mu = \eta I \tag{2.47}$$

Where I represent spin and η is the gyromagnetic ratio, a proportionality constant the relation between the angular momentum and the magnetic dipole moment, specific to each nucleus which is represented in Table 2.3.

Table 2.3. NMR (D): The gyromagnetic ratios for some common nuclei.

Nuclei	**Spin**	**Gyromagnetic Ratio (MHz/T)**	**Natural Abundance (%)**
^{1}H	1/2	17.235	99.9985
^{13}C	1/2	10.705	1.07
^{31}P	1/2	17.235	100
^{27}Al	5/2	11.103	100
^{23}Na	3/2	11.262	100
^{7}Li	3/2	16.546	92.41
^{29}Si	1/2	-8.465	4.68
^{17}O	5/2	5.772	0.038
^{15}N	1/2	-4.361	0.368

The Zeeman Hamiltonian for a spin with the quantum number I in a magnetic field is:

$$H = -\frac{\eta h B_o I}{2\pi} \tag{2.48}$$

Where B_o is the magnetic field, the energy levels divided into (2I + 1) sublevels for a spin I under the influence of a fixed magnetic field. Which are represented in Figure 2.6, the energy difference can be expressed between adjacent levels by:

$$\Delta E = -\frac{\eta h B_o m_l}{2\pi} \tag{2.49}$$

Where m_l takes values $\pm I, \pm(I-1), \ldots \pm 1/2$. When It is a half-odd integer or an integer.

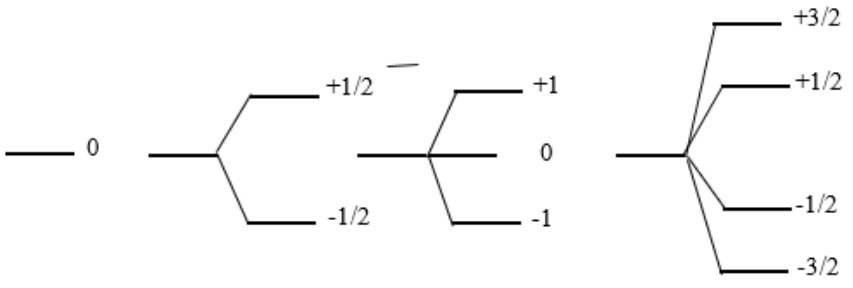

Figure 2.6. The energy level splits into (2I +1) levels under the effect of a magnetic field.

Larmor frequency of the isotope in the field of Bo is a constant value= $\frac{\eta h B_o}{2\pi}$, which generally can be expressed in the frequency unit that Zeeman energy levels are shown. This frequency of resonance varies in direct proportion to the field applied, means the large the magnetic field cause the higher the resonance frequency. Which are represented in Figure 2.7.

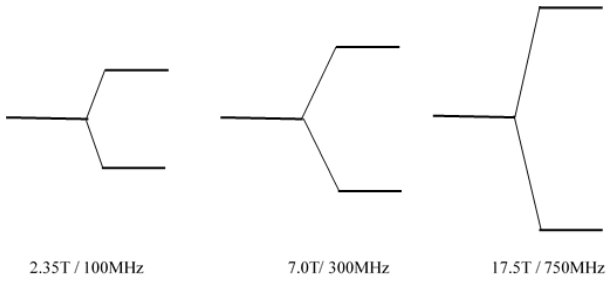

Figure 2.7. The energy difference between two neighboring levels.

2.4. Experimental Details

Anthra [2, 3-B: 6, 7-B'] Dithiophene (ADT) molecule, dichloromethane (DCM), chloroform (CHF) and N,N-Dimethylacetamide (DMAC) solvents were purchased from Sigma-Aldrich Company. Firstly, we weighed three equally-mass ADT molecules using the AND-GR-200 Series Analytical Balance to dissolve in these three different solvents. These ADT molecules were dissolved in 13 mL of the respective solvents. The prepared solutions were mixed with a stirrer (FOUR E'S Scientific) for 5 minutes. Then, these solutions, which did not seem to dissolve very well, were placed on a hot-plate (Heidolph) for 10 minutes. Thus, very well dissolved ADT solutions were prepared.

The UV and FTIR measurements of the ADT solutions for DCM, CHF and DMAC solvents at room temperature were performed using the UV spectrophotometer (Shimadzu-1800) and using the Perkin Elmer 65 Spectrum with KBr pellet, respectively.

3. RESULTS AND DISCUSSION

These theories that given in this thesis were applied to molecules of Anthra [2, 3-b: 6, 7-b'] Dithiophene (ADT). The atomic configuration for ADT molecule consists of two sulfur atoms, ten hydrogen, and eighteen carbon atoms, as shown in this Figure 3.1. In this thesis, we obtained FTIR, UV, and NMR, also we have investigated the band-gap energy in different ways. All computational were suitable methods with suitable basis sets after used many different methods with optimization.

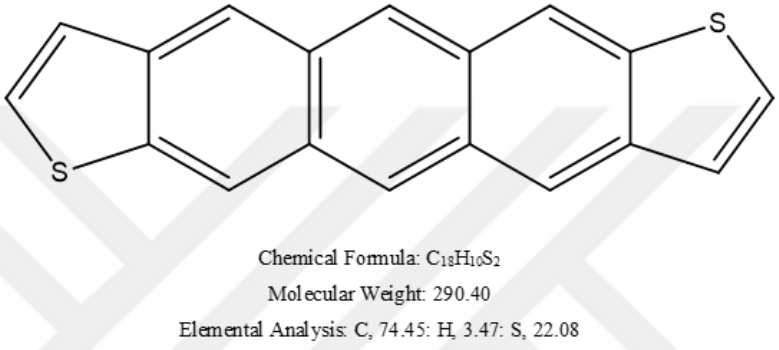

Figure 3.1. Molecular structure of Anthra [2, 3-b: 6, 7-b'] dithiophene (ADT) [42].

The ADT molecule has four different bonds, such as carbon-carbon single bond (C-C), carbon-carbon double bond (C=C), carbon-hydrogen bond (C-H) and carbon-sulfur bond (C-S). Anthradithiophene is a front-runner in the world of small molecule semiconductors (SMS) for organic electronics and photo electronics. It is aromatic and usually non-polar and non-miscible with water. Also due to its low ration of hydrogen to carbon, as shown in that Figure 3.1, it is beneficial as solvents for other non-polar compounds. O. Kwon and co-workers have shown that ADT, the intrinsic electronic structure, the relevant intermolecular interaction, and the intramolecular vibrational modes are very comparable to those in pentacene [40]. Also, they indicated that the first ionization of Anthra [2, 3-b: 6, 7-b'] dithiophene has an energy of vertical is around 6.6996 eV and the anti-ADT is more stable than the syn-ADT by nearly 0.02 kcal/mole. In addition, they determined the ionization potential [41] of ADT is slightly higher than pentacene and lower than the experimental value by nearly 0.6 eV, the IP of ADT is calculated to be 6.15 eV and the ADT has a small reorganization energy (0.094eV), which is equivalent to pentacene [42].

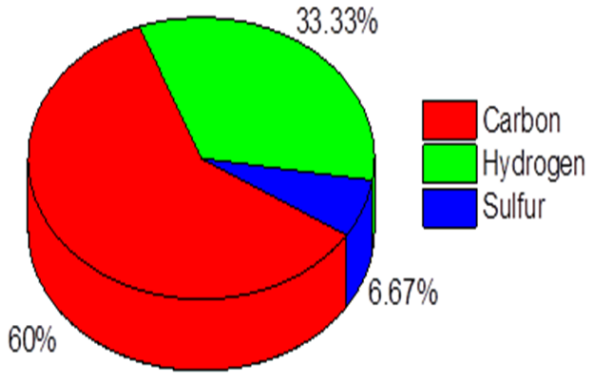

Figure 3.2. Conformation of Anthradithiophene by elements (gram/mole) [54].

The angular anthradithiophene (a-ADT) molecules have the low-lying HOMO level (-4.81 eV), also LUMO level is calculated to be -2.02 eV, the band-gap energy is estimated to be 2.79 eV. The ADT indicates great oxidation stability in OFET devices due to low-lying HOMO level and the implementations of OFETs [42-50]. The high mobilities observed in this series indicate a great potential for their use in practical applications. Anthra [2, 3-b: 6, 7-b'] dithiophene is a p-type small molecule. It has been proving to appearance good crystallinity, also high mobilities of less than one cm2/Vs in solution-processed organic field-effect transistors. Therefore, it is a broadly used material for the building of organic field-effect transistors [51]. Due to HM of ADT, the functionalized ADT derivatives have been attracting considerable attention [52]. The hole mobility in ADT single crystals nearly increases with decreasing temperature following a power law ($\mu \propto T^{-n}$) [53, 54].

Some researchers used the anthradithiophene-donor unit and aforesaid acceptor units to synthesize corresponding copolymers to explore their photovoltaic performance [53, 55]. ADT was manufactured as reported earlier. Thin (ten micrometers) sized platelets of ADT single crystals were grown from the vapor phase in a stream of gas [56]. J. H. Schön and co-workers [54] have shown that the properties of the ADT is a small organic molecule and charge transport dependence of temperature, in the layered p-type, the mobility for in-plane transport displays an inverse power law temperature. The ADT was initially synthesized as the mixture of anti-isomer and syn-isomer due to a complications with isomer departure [57].

In the final, the ADT is a diverse molecule that can be made to order to a suitable different type of electronic application such as organic photovoltaics and organic field-effect transistors and it is isostructural and isoelectronic of pentacene [58].

3.1. Optimization of ADT

In this thesis, we used two different methods like the DFT and HF theory with some of the basis sets such as 3-21G, 6-31G, 6-31G (d, p), 6-311G, LanL2DZ, and SDD. The ADT molecule was optimized before starting quantum mechanical computation, as shown in Figure 3.3. After optimization, all of the basis sets, as shown in the Table 3.1, we used suitable theory with suitable basis sets, for all computational FTIR, UV, and NMR, and determined the band-gap.

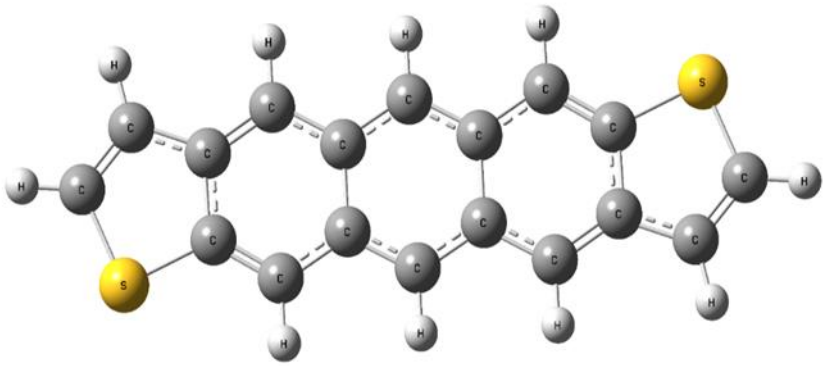

Figure 3.3. Optimization of ADT molecule made by GaussView 9.

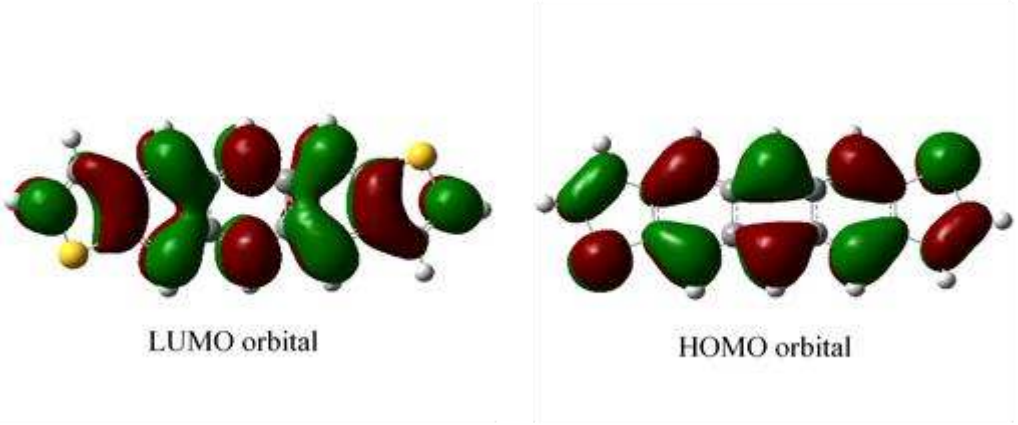

Figure 3.4. The energy levels for HOMO and LUMO orbitals of C_{18} H_{10} S_2.

Figure 3.4 indicates the Highest Occupied Molecular Orbital (HOMO) and the Lowest Unoccupied Molecular Orbital (LUMO). The result of all the value of the energy band-gap for different theory with various the basis sets is shown in Table 3.1.

Table 3.1: The different Band-Gap by DFT and HF theory for many basis sets.

Basis Sets		**HF**	**DFT**
6-21G	LUMO	1.160 eV	-0.672 eV
	Band gap=	8.010 eV	1.431 eV
	HOMO	-6.850 eV	-2.103 eV
6-31G	LUMO	1.184 eV	-2.067 eV
	Band gap=	7.881 eV	2.902 eV.
	HOMO	-6.697 eV	-4.969 eV.
6-31G(d, p)	LUMO	1.330 eV	-2.024 eV
	Band gap=	7.833 eV.	2.785 eV
	HOMO	-6.503 eV	-4.809 eV
6-311G	LUMO	1.015 eV	-2.299 eV
	Band gap=	7.840 eV	2.890 eV.
	HOMO	-6.825 eV	-5.189 eV
LanL2DZ	LUMO	0.893 eV	-2.284 eV
	Band gap=	7.720 eV	2.829 eV
	HOMO	-6.827 eV	-5.113 eV
SDD	LUMO	0.915 eV	-2.271 eV
	Band gap=	7.732 eV	2.824 eV
	HOMO	-6.817 eV.	-5.095 eV

In experimental data, we determined the value of the band-gap energy between 2.4 eV to 2.9 eV. Firstly, both methods (DFT and HF theory) were used for optimization with some basis sets as shown in this Table 3.1. These results show that the DFT theory is much better than the HF theory, on the other hand, the HF theory is not working for the ADT molecule.

3.2. Electrostatic Potential Map of ADT

Figure 3.5 shows the Potential Energy Surfaces (PES), also it illustrates the region of colors. The red region corresponds to the region of greatest electron density. It means that the red region of this diagram corresponds to the region of greatest electronegativity. Also, the blue color represents a small electronegativity. About yellow and green color, they have more electronegativity than blue and less than red color, the yellow color is more electronegativity than green color. Recall that the area of lowest electrostatic potential corresponds to the area of greatest electron concentration. Around of sulfur have more electronegativity comparing with another region. As well as, around of all hydrogens have less electronegativity comparing with another region. The Potential Energy Surfaces (PES) of ADT molecule in the Figure 3.5.

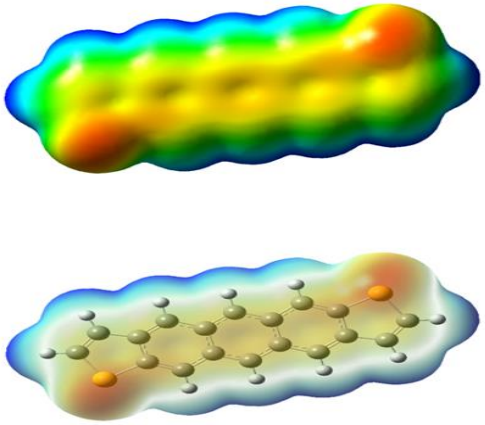

Figure 3.5. The Potential Energy Surfaces (PES) of ADT molecule.

In the end, the sulfurs have the greatest electronegativity value and the hydrogens have the smallest electronegativity value. On the other hand, the sulfur would be affiliated with the red region of the diagram, and the hydrogen would be affiliated with the blue region.

3.3. Applying IR Spectroscopy on the ADT Organic Semiconductor

The vibration frequency (VF) of the ADT molecule was calculated by using the DFT method of B3LYP with some basis sets such as 6-31G, 6-31G (d, p), 6-311G, LanL2DZ, and SDD. The vibrational band projects were generated using the Gauss-View 09 visualization program. Also, these were compared with each basis sets.

The method IR spectroscopy is very useful for determining functional groups in the Table 3.2. Figure 3.6 shows the IR absorbance spectra of the ADT molecule for basis set (6-31G). If we take

the signals and estimate that the present transmittance is around eighty percent that means that the twenty percent of that energy was absorbed and eighty percent passed through the sample. It is clear that the relationship between absorbance and transmittance are inversely related. Typically, the existence of one or more aromatic rings in a structure is effortlessly determined from the carbon-carbon double bond (C=C) and carbon-hydrogen bond (C-H) related vibration. As shown the ADT molecular has four bounds such as carbon-carbon single bond (C-C), carbon-carbon double bond (C=C), carbon-hydrogen bond (C-H) and carbon-sulfur single bond (C-S). The important range in the IR absorption is the functional groups that the more the evidence takes placed. The functional group region appears nearly from 1300 to 4000 wavenumber of reciprocal centimeters. Also, the IR absorption has the fingerprint region that it appears nearly from 400 to 1300 wavenumber of reciprocal centimeters. There are two forms in which vibrations can happen such as bending and stretching, bending for the same bond is much lesser since there is less resistance. A very significant notice is that vibration is IR active only if in dipole moment it causes a net change.

Table 3.2. Characteristic IR absorption frequencies of organic functional groups.

Aromatic		
Group	Appearance	Absorption (cm^{-1})
C=C Bending	medium	1700 - 1500
C=C Stretch	medium-weak, multiple bands	1400-1600
C-C Stretch (in-ring)		1585-1600
C-H Stretch		3000-3300
C-H Bending	Weak "overtones"	1650-2000
C-H Bending	out-of-plane "oop"	900-675
C-H Bending	in-plane Weak	1250-1000
C-S Stretch		690-685

Table 3.2 gives information about IR absorption frequencies for various group functional, these values are shown for these group functional that indicated. They sued for comparing with expectation data and simulation program.

The existence of four bonds in a structure is typically determined from the C-C, C=C, C-H, and C-S structure related vibrations. The IR absorbance spectra of the ADT molecule for basis set (6-31G) in Figure 3.6. The carbon-hydrogen stretching vibration takes place between the 3000 cm^{-1} and 3300 cm^{-1} and is usually displayed a multiply weak peak. The C-H stretching is observed at around 3200 cm^{-1} as seen in Figure 3.6. The aromatic C-H in-plane bending, out-of-plane bending and weak bending occur between 1250 cm^{-1} -1000 cm^{-1}, 900 cm^{-1} - 675 cm^{-1} and 1650 cm^{-1} -2000 cm^{-1}, respectively. But the C-H bending is observed at around 1000 cm^{-1} in-plane, at 920 cm^{-1} in out-of-plane and C-H weak bending is observed at around 1650 cm^{-1}. The C-C stretching in-ring and C-S stretching are observed at nearly 1600 cm^{-1} and 650 cm^{-1}, respectively. The theoretically calculated value by DFT with B3LYP methods displays a suitable with registered value in Table 3.2.

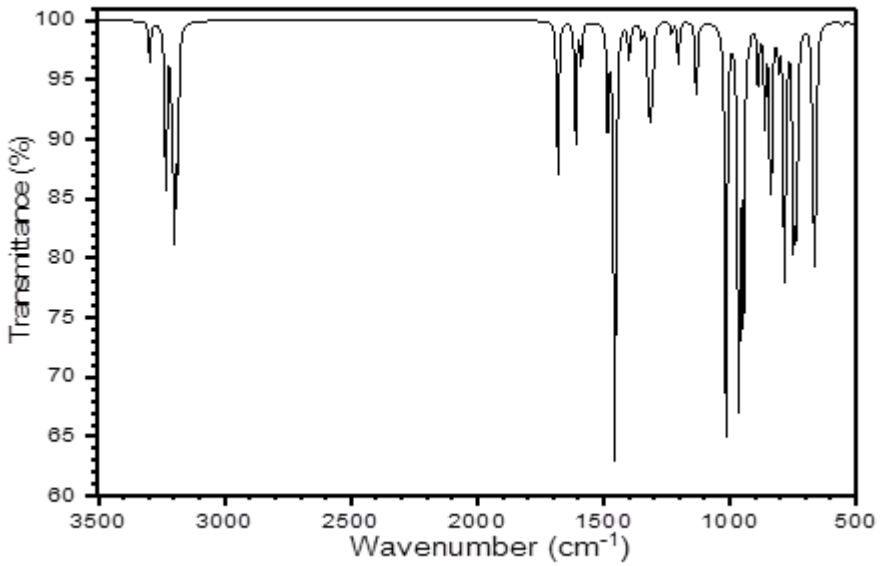

Figure 3.6. The IR absorbance spectra of the ADT molecule for basis set (6-31G).

Figure 3.7 shows all of the peaks, which are indicated slightly different by comparing with the peaks of Figure 3.6. For example, the C-H stretching is observed nearly less at 3200 cm^{-1}, comparing with the peaks of Figure 3.6, also the transmittance is nearly eighty percent but in Figure 3.7 transmittance is nearly eighty-five percent. The aromatic C-H in-plane bending, out-of-plane bending and weak bending are observed slightly less than 1000 cm^{-1} in plane, 910 cm^{-1} in out-of-plane, finally, the C-H weak bending is observed at around 1610 cm^{-1}. The C-C stretching in-ring and C-S stretching are observed at nearly 1640 cm^{-1} and 620 cm^{-1}, respectively. The theoretically calculated value by DFT with B3LYP methods using the basis set (**6-31G(d, p)**) display a suitable

with registered value in Table 3.2.

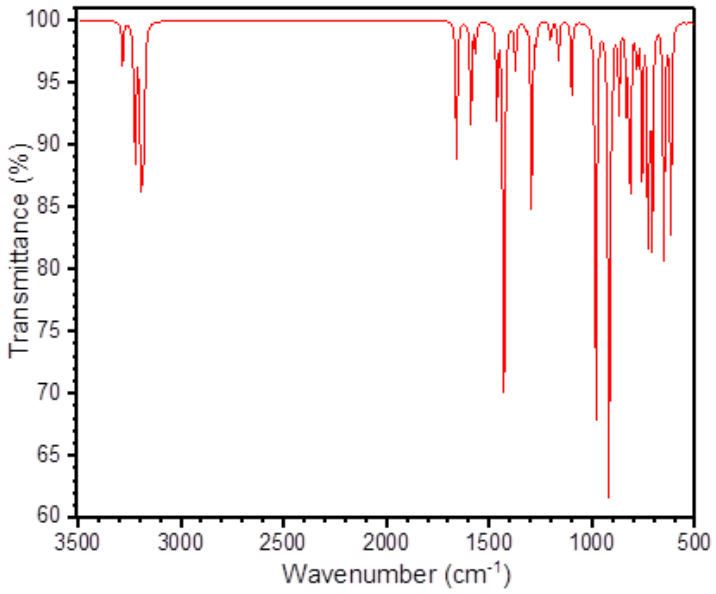

Figure 3.7. The IR absorbance spectra of the ADT molecule for basis set (6-31G (d p))

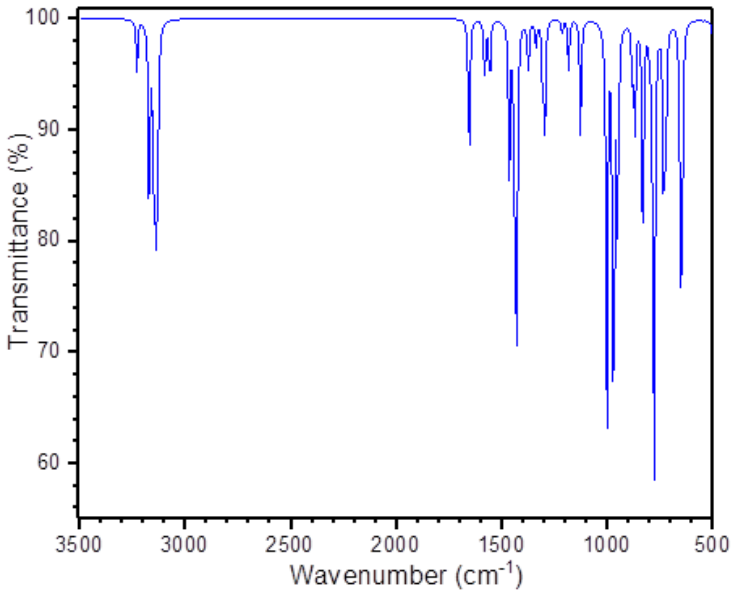

Figure 3.8. The IR absorbance spectra of the ADT molecule for basis set (6-311G).

Figure 3.8 shows the IR absorbance spectra of the ADT molecule for basis set (6-311G). In general, the peak of C-H stretching slightly less passed through the sample compared with using

the basis set (**6-31G(d,p)**) and is vice versa with using the basis set (**6-31G**). The C-H stretching is observed nearly less at 3100 cm-1. The aromatic C-H in-plane bending, out-of-plane bending and weak bending are observed slightly less than 1000 cm^{-1} in plane the same as with using the basis set (**6-31G(d,p)**),but less passed through the sample comparing with it, 9500 cm^{-1} in out-of-plane the same as with using the basis set (**6-31G**), finally, the C-H weak bending is observed at around 1600 cm^{-1} the same as with using the basis set (**6-31G**). The C-C stretching in-ring and C-S stretching are observed at 1560 cm^{-1} and 600 cm^{-1}, respectively. The theoretically calculated value with B3LYP methods for basis set (**6-311G**) displays a suitable with registered value in Table 3.2.

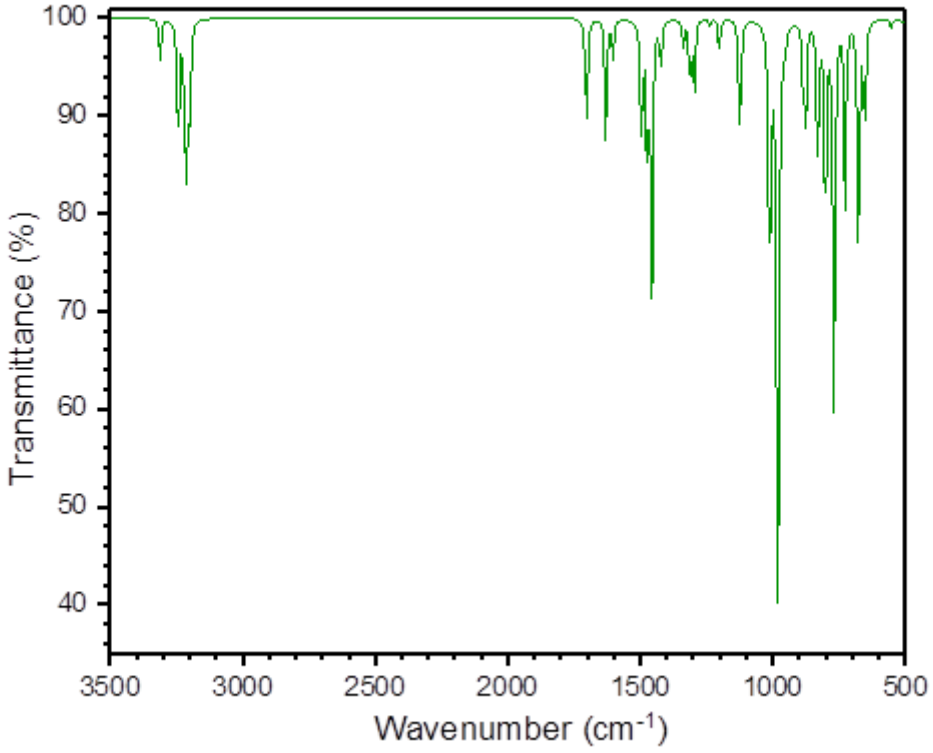

Figure 3.9. The IR absorbance spectra of the ADT molecule for basis set (Lanl2dz).

Figure 3.9 indicates the IR absorbance spectra of the ADT molecule for basis set (Lanl2dz). The peak of C-H in-plane bending indicates that the value of transmittance is forty percent by comparing with the using these basis sets such as (6-31G), (6-31G(d,p)) and (6-311G). The C-H stretching is observed nearly less at 3200 cm-1. The aromatic C-H in-plane bending, out-of-plane bending and weak bending are observed slightly less than 1000 cm^{-1} in plane the same as with using the basis sets (6-31G(d,p)) and (6-311G), 850 cm^{-1} in out-of-plane less than comparing with basis sets (6-31G), (6-31G(d,p)) and (6-311G), finally, the C-H weak bending is observed at around 1600

cm^{-1} the same as with using the basis sets (6-31G) and (6-311G). The C-C stretching in-ring and C-S stretching are observed at less than 1500 cm^{-1} and 750 cm^{-1}, respectively. The theoretically calculated value with B3LYP methods for basis set (Lanl2dz) displays a more suitable with registered value in Table 3.2.

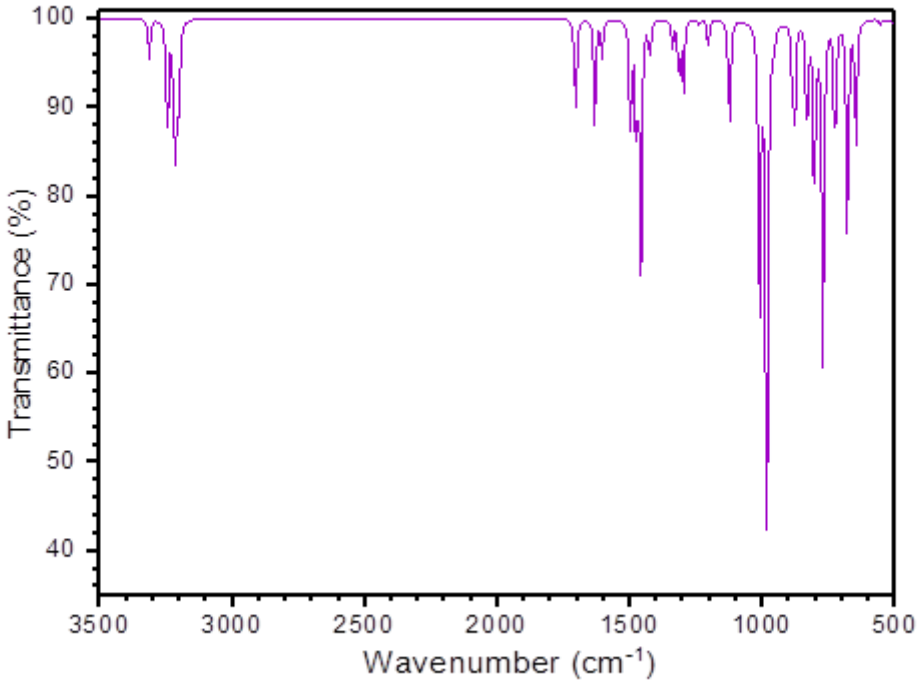

Figure 3.10. The IR absorbance spectra of the ADT molecule for basis set (DSS).

Figure 3.10 shows the IR absorbance spectra of the ADT molecule for basis set (DSS). All of the peaks nearly are the same with using basis set (Lanl2dz), until about transmittance except same of peaks different about passed through the sample, such as C-H out-of-plane bending, weak bending, and C-S stretching. The C-H stretching is observed nearly around at 3300 cm^{-1}. About the aromatic C-H in-plane bending, out-of-plane bending and weak bending are observed at 980 cm^{-1} in plane approximating with using the basis set (6-311G) 730 cm^{-1} in out-of-plane less than comparing with basis set (Lanl2dz), finally, the C-H weak bending is observed at around 1600 cm^{-1} the same as with using the basis set (Lanl2dz). The C-C stretching in-ring and C-S stretching are observed at less than1500 cm^{-1} and 730 cm^{-1}, respectively. The theoretically calculated value with B3LYP methods for basis set (DSS) displays a more suitable with expectation value in Table 3.2, comparing with another basis sets.

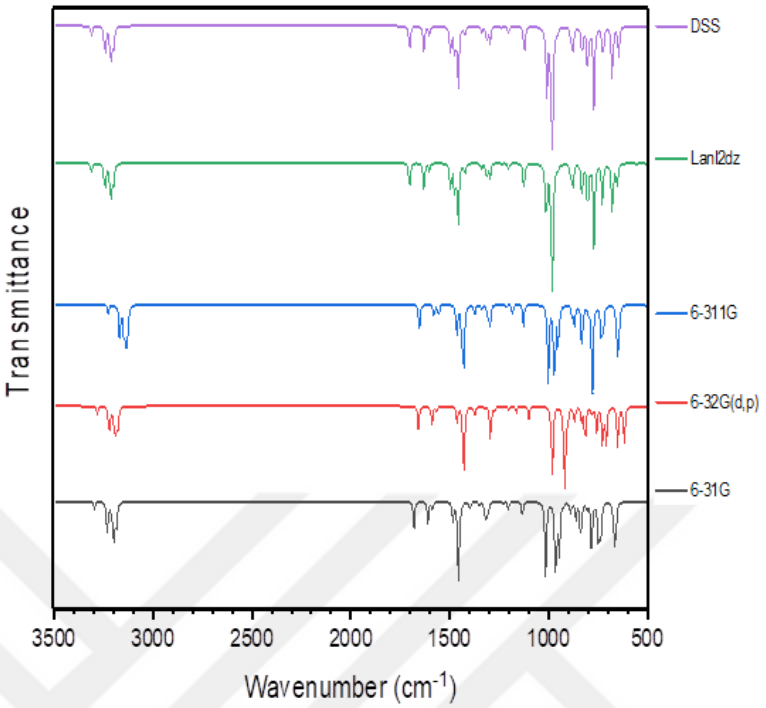

Figure 3.11. The IR absorbance spectra of the ADT molecule for some basis sets.

Figure 3.11 shows the different IR absorbance spectra by using different basis sets. The x-axes represent the wavenumber and the y-axes represent the transmittance. Also, this Figure indicates the important part which did not occur the absorption. This part did not occur the absorption between 1650 cm^{-1} and 3200 cm^{-1}. These results show that all of the basis sets are nearly the same. In the end, the absorption of the IR radiation in the ADT molecule was not occurred the range between the 1650 cm^{-1} and 3200 cm^{-1}.

3.4. The Electronic and Optical Studies of The Explanations of The ADT Molecule

UV spectroscopy and UV visible spectroscopy were probably the first method used by chemists to discover the atomic structure and then later molecular structure. On the other hand, it is easiest optical techniques to examine the optical and electronic properties of the particles in the range of nano. Figure 3.9 indicates the absorbance spectra of the ADT molecule for basis set 6-31G. As shown in Figure 3.12, the absorption wavelength is occurred at 224 nm, 227 nm, and 477 nm. They are called λ_M "lambda maximum". They are colorless, these absorptions are occurred at 224 nm and 227 nm. The ADT molecule has many carbons, each one is SP^2 hybridized that means each one of those carbons has a π-orbital. The reason why ADT has a color is that it absorbs light in the visible region of the electromagnetic spectrum. The visible region starts at approximately

400 nanometers, and less than 400 nm would be the UV, it seems that the ADT molecule, wavelength absorbed approximately 477 nanometers for this absorbs in the visible region. The visible region goes to around 700 nm. Also, above the 700 nm is called infrared (IR) region on the ES.

The ADT molecule absorbed the blue-light wavelength the range approximation 477 nm, it means that the color appears orange light, as shown in Figure 3.12. This transition occurred from non-bonding orbitals to π*-antibonding orbitals. A π*-antibonding orbital needs less energy, it means absorb light of a higher wavelength and a lower wavelength. In the end, Table 3.3 gives information about these energies which occurred by different absorbance due to different transitions from π-bonding to π*-antibonding and from none-bonding to π*-antibonding.

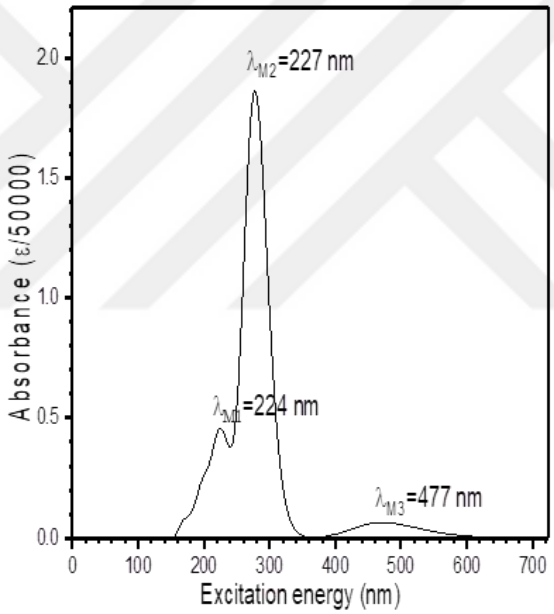

Figure 3.12. The absorbance spectra of the ADT molecule for basis set 6-31G.

Figure 3.12 indicates the absorbance spectra and many peaks of the ADT molecule for basis set 6-31G. These peaks indicate different transitions from π-bonding to π*-antibonding and from none-bonding to π*-antibonding. In these peaks, just this peak at 477 nm indicates the color of the ADT molecule since this absorption is observed in the visible region. Other peaks such as 224 nm and 227 nm are not observed, since these absorptions are observed in the UV region. The energy of the peak of 477 nm is 2.6 eV, it is approximation with using HOMO and LUMO orbitals for determining the band-gap, by using this formula, $E=hc/\lambda$.

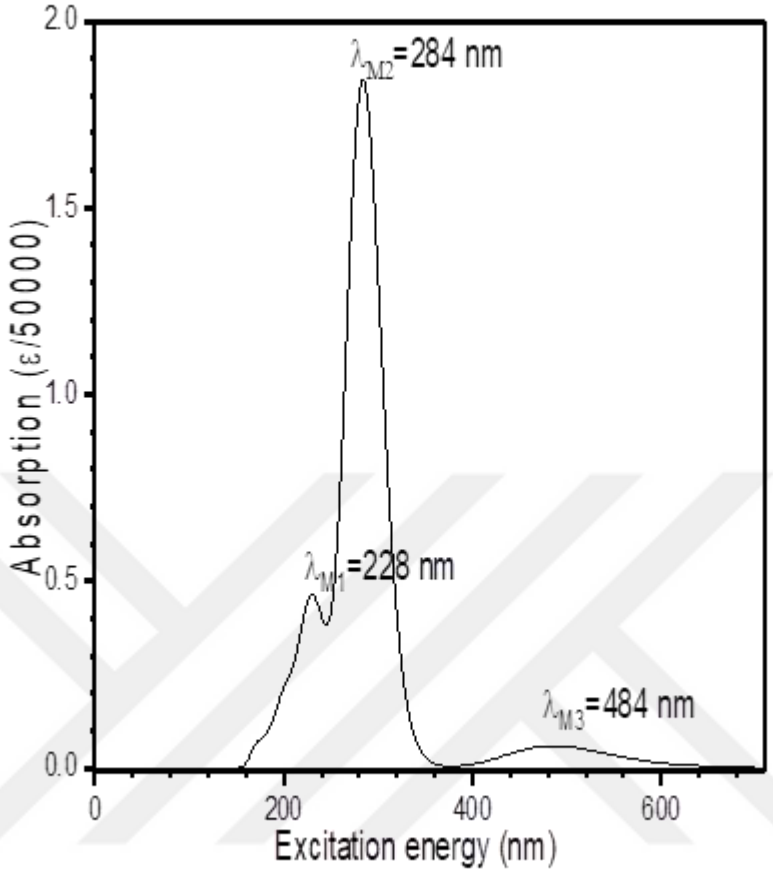

Figure 3.13. The absorbance spectra of the ADT molecule for basis set 6-31G (d, p).

Figure 3.13 indicates the absorbance spectra and many peaks of the ADT molecule for basis set 6-31G (d, p). In this Figure, the peak of 484 nm indicates the color of the ADT molecule since this absorption is occurred in the visible region. Other peaks such as 228 nm and 284 nm are not observed since this absorption is occurred in the UV region, at the same with using the basis set 6-31G. The energy of the peak of 484 nm is 2.56 eV, it is approximation with using HOMO and LUMO orbitals for determining the band-gap, by using this formula, $E=hc/\lambda$.

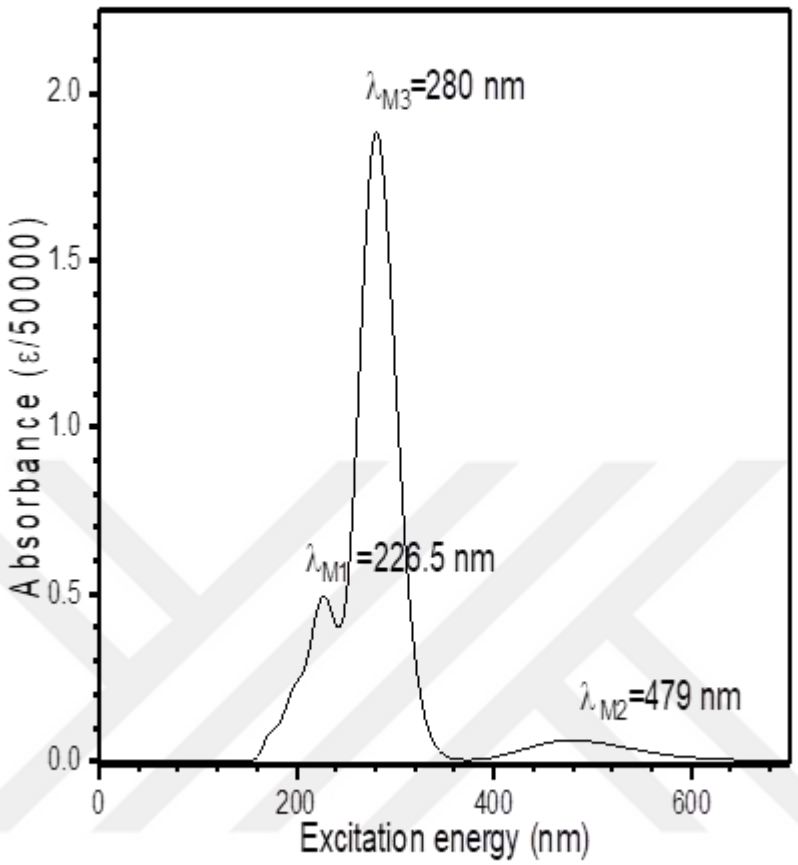

Figure 3.14. The absorbance spectra of the ADT molecule for basis set 6-311G.

Figure 3.14 the absorbance spectra and many peaks of the ADT molecule for basis set 6-311G. In this Figure, the peak of 479 nm indicates the color of the ADT molecule since this absorption is occurred in the visible region. Other peaks such as 226.5 nm and 280 nm are not observed since these absorptions are occurred in the UV region, they are approximation with using the basis set 6-31G (d, p). The energy of the peak of 479 nm is 2.59 eV, it is close comparing with using the basis set 6-31G, also it is approximation with using HOMO and LUMO orbitals for determining the band-gap.

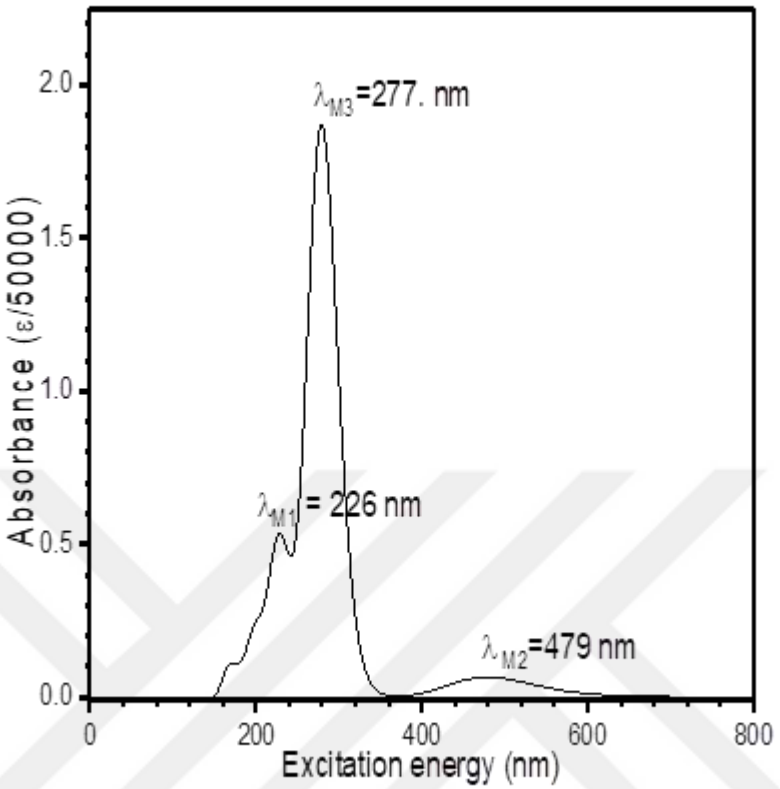

Figure 3.15. The absorbance spectra of the ADT molecule for basis set LanL2DZ.

Figure 3.15 shows the absorbance spectra and many peaks of the ADT molecule for basis set LanL2DZ. All peaks are approximation with using the basis set 6-311G. In this Figure, the peak of 479 nm indicates the color of the ADT molecule since this absorption is occurred in the visible region. Other peaks such as 226. nm and 277 nm are not observed since these absorptions are occurred in the UV region. The energy of the peak of 479 nm is 2.59 eV, it is close comparing with using the basis set 6-311G, also it is fixed with using HOMO and LUMO orbitals for determining the band-gap.

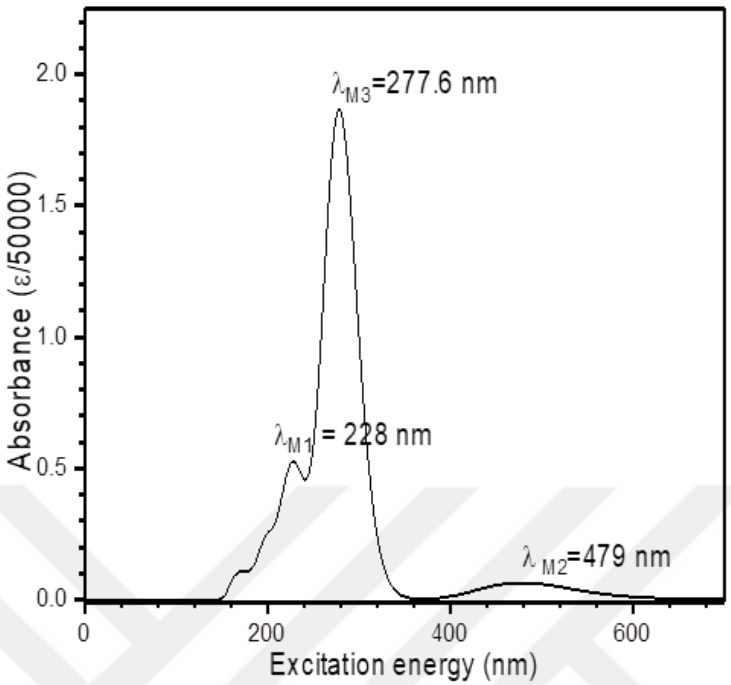

Figure 3.16. The absorbance spectra of the ADT molecule for basis set DSS.

Figure 3.16 indicates the absorbance spectra and many peaks of the ADT molecule for basis set DSS. All peaks are approximation with using the basis set LanL2DZ. In this Figure, the peak of 479 nm indicates the color of the ADT molecule. Other peaks such as 228 nm and 277.6 nm are not observed since these absorptions are occurred in the UV region, The energy of the peak of 479 nm is 2.59 eV, it is the same with using the basis sets {6-311G and LanL2DZ}, also it is fixed with using HOMO and LUMO orbitals for determining the band-gap.

Above figures indicate band gap (E_g) obtained by using the DFT with different basis sets such as 6-31G, 6-31G (d, p), 6-311G, LanL2DZ and DSS for compared in different way to know which way is best for determining the E_g. Also, all results are determined in Table 3.3.

Table 3.3. Determining different band-gap with different basis sets.

DFT			
Basis Sets	**Maximum Wavenumbers (nm)**		**Band Gap Energy (eV)**
6-31G	λ_{M1} =	224	5.54
	λ_{M2} =	227	5.46
	λ_{M3} =	477	2.60
6-31G(d, p)	λ_{M1} =	228	5.44
	λ_{M2} =	284	4.37
	λ_{M3} =	484	2.56
6-311G	λ_{M1} =	226.5	5.48
	λ_{M2} =	280	4.43
	λ_{M3} =	479	2.59
LanL2DZ	λ_{M1} =	226	5.49
	λ_{M2} =	277	4.49
	λ_{M3} =	479	2.59
SDD	λ_{M1} =	228	4.30
	λ_{M2} =	277.6	4.47
	λ_{M3} =	479	2.59

3.5. Determination of Band Gaps by Using Tauc/Davis–Mott Model

When light put on a semiconductor surface is partially transmitted and partially reflected. Absorption can be determined from the perspective of the absorption coefficient on the energy, E_g is valued using the following relation.

$$(\sigma h\nu)^{\frac{1}{n}} = A(h\nu - E_g) \tag{3.1}$$

This equation is known as Tauc and Davis-Mott relation. In this equation, σ represent the absorption coefficient, **h,** and **v** represent the constant of Planck and frequency of the photon, respectively. Also ”hv” is called incident photon energy, **A** is constant, $\mathbf{E_g}$ represent the optical band gap energy of nanomaterial and the exponent “n” represent the nature of transition. The value of the “n” indicates the behavior of transition such as the direct allowed, indirect allowed, direct

forbidden and indirect forbidden transition. For example, when the n is equal to two, it represents indirect allowed transition, the n is equal to half, it represents direct allowed transition, the n is equal to three, it represents indirect forbidden transition and the n is equal to three over three, it represents direct forbidden transition. The plots of the$(\sigma h\nu)^{\frac{1}{n}}$, versus energy (E), with different the value parameter "n": n=2, 1/2, of the ADT semiconductor, when n= 2 and 1/2. The direct and indirect allowed band gap value were achieved from linear regions of in all figures above in these subsections, they also indicate the energy band-gap, using the different nature of the transition to indicate which provides the better suitable and then identifies the correct transition type. In the end, all the results indicate the correct transition type. The ADT molecule has the direct allowed transition as shown in Figure 3.17.

Figure 3.17 shows the energy band-gap with using different the nature of transition. It is important for knowing which one provides the better fit and thus identifies the correct transition type. Figure 3.17 shows correct transition type when used n is equal a half since it is suitable and closing with the expectation value.

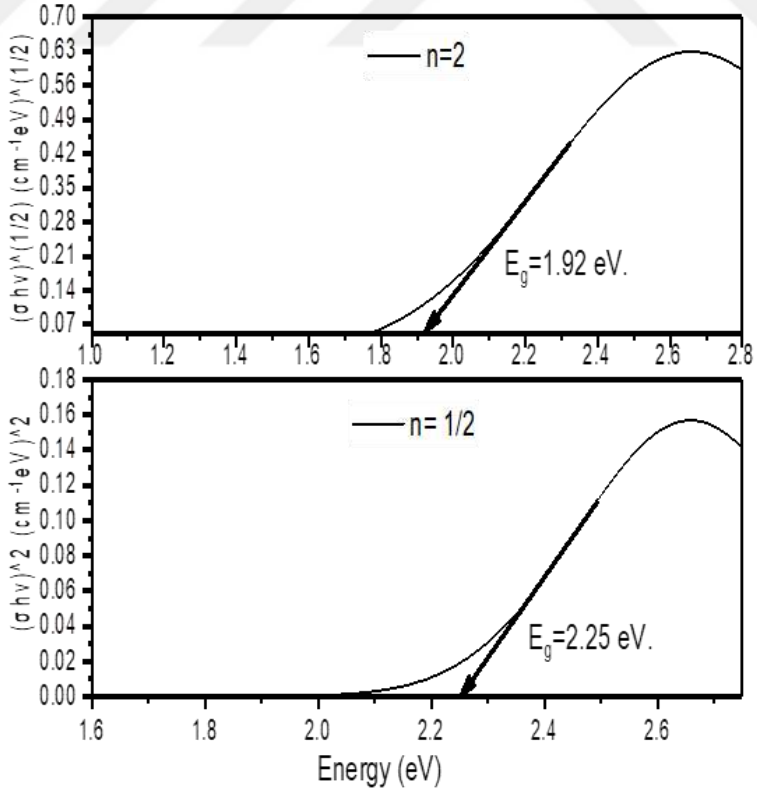

Figure 3.17. Optical energy of ADT for basis set, 6-31G got from the Tauc plot.

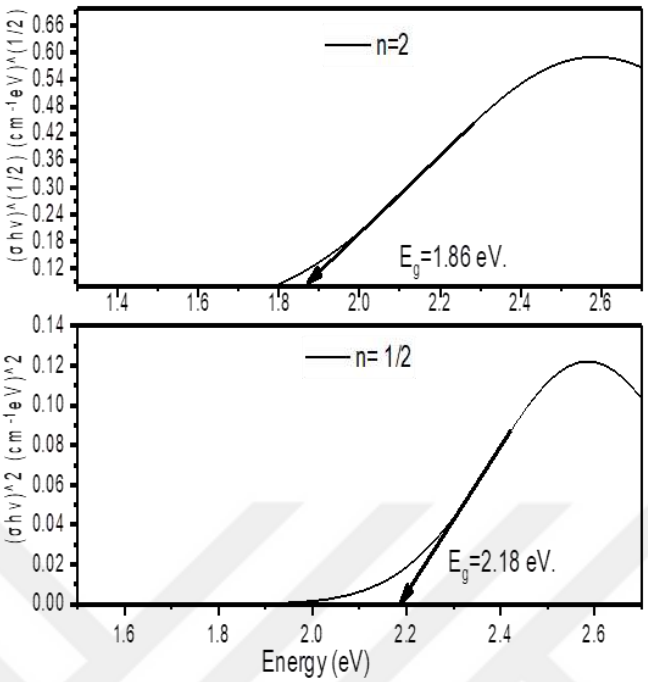

Figure 3.18. Optical energy of ADT for basis set 6-31G (d, p), got from the Tauc plot

Figure 3.18 also shows the energy band-gap with using different the nature of transition. Figure 3.18 indicates the correct transition type when used n is equal a half, since it is suitable and closing with the expectation value, as the same as with using the basis set (6-31G).

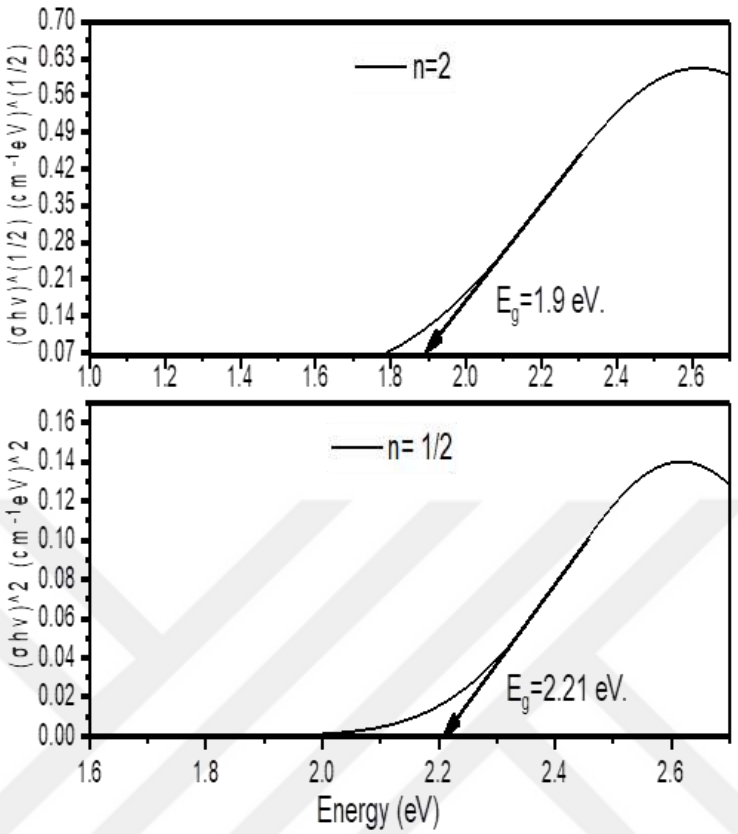

Figure 3.19. Optical energy of ADT for basis set, 6-311G got from the Tauc plot.

Figure 3.19 shows the band-gap by using the different basis set (6-311G), to know surely the correct transition type with using the different nature of the transition. At the end, these results show that the ADT molecule has the direct allowed transition, as the same as with using the basis sets {6-31G and 6-31G (d, p)}.

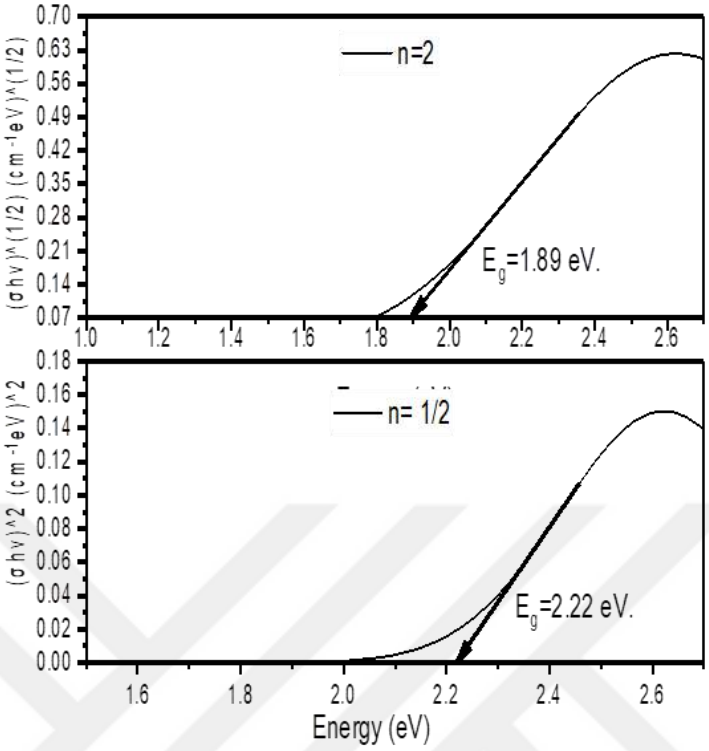

Figure 3.20. Optical energy of ADT for basis set, LanL2DZ got from the Tauc plot

Figure 3.20 shows the energy band-gap with use different the nature of transition. They indicated that the ADT molecule has the direct allowed transition since the value of band-gap is equal to 2.22 eV, it is suitable and closing with the expectation value when used n is equal a half.

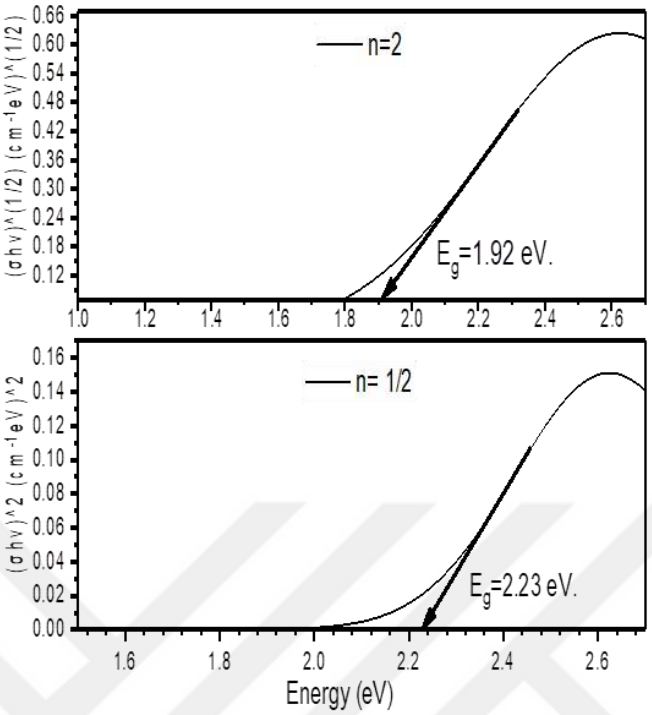

Figure 3.21. Optical energy of ADT for basis set, DSS got from the Tauc plot.

Figure 3.21 also shows the band-gap (E_g) with using different the natural of transition.as well as, in this Figure as the same as by using another basis sets {(6-31G), (6-31G (d, p)), {(6-311G) and (LanL2DZ)}. Obtained results indicated that the ADT molecule has the direct allowed transition. Above figures indicate band gap (E_g) by different methods for compared in a different way to know which way is best for determining the E_g. Also all results are determined in Table 3.4. After all result, the band-gap of the ADT molecule indicated that it has a direct allowed band-gap. It means the transitions of electron direct translate from valance band to the conduction band.

Table 3.4. Determining different band-gap energy (Eg) using the different nature of the transition.

DFT		
Basis Sets	**E_g (eV) for n=2**	**E_g (eV) for n=1/2**
6-31G	1.92	2.25
6-31G(d, p)	1.86	2.18
6-311G	1.9	2.21
LanL2DZ	1.89	2.22
SDD	1.92	2.23

Table 3.4 shows information about the energy gap with different basis sets and for each basis sets using two types of natural transition such as n=2 and n=1/2. It is noticeable that when using the n is equal to two, the average energy band gap is equal to 1.898 eV by using five basis sets. As well as, when n is equal half, the average band-gap is equal to 2.218 eV by using five basis sets. It is clear that by using n=1/2, is more suitable with the expectation value, in the result indicated that this ADT have direct allowed band-gap, it is important to know, since when the molecules have direct allowed band-gap, they get information that when electron rises from valence band to the conduction band will only change it is potential energy. As well, when the molecule has indirect allowed band-gap, they get information that when electron rises from valence band to the conduction band will only change it is potential energy and momentum.

3.6. Experimental FTIR Results for ADT Molecule

Figure 3.22 shows the FT-IR spectra of the ADT molecule for DCM, CHF and DMAC solvents. The FT-IR spectrum of the bands at about 2355 cm^{-1} for these solvents gives a strong peak, which shows the strong C-H stretching. The IR spectrum band at 1693 cm^{-1} for DMAC solvent corresponds to hydrogen bonding. The IR spectrum band at 1402 cm^{-1} for DMAC solvent shows the δC-H_3. The IR spectrum band at 1219 cm^{-1} for CHF solvent indicates the CH_2 and CH_3 groups. The IR spectrum band at 772 cm^{-1} for CHF solvent indicates the strong C-C stretching. The IR spectrum band at about 750 cm^{-1} for CHF and DCM solvents shows the C-H bending. The IR spectrum band at about 668 cm-1 for CHF and DCM solvents shows the C-S stretching.

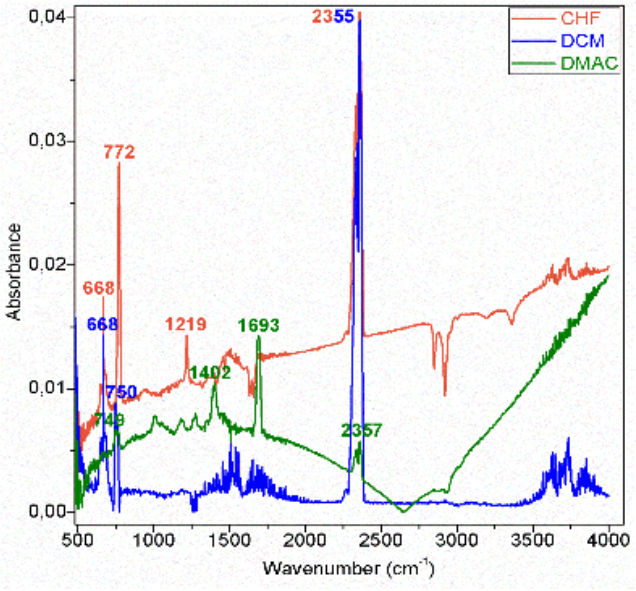

Figure 3.22. The FT-IR spectra of the ADT molecule for DCM, CHF and DMAC solvents.

3.7. Experimental UV Spectra Results for ADT Molecule

We recorded the UV-Vis spectra of the ADT molecule for DCM, CHF and DMAC solvents. Absorbance is important for optoelectronic applications. Fig. 3.23 indicates the absorbance spectra of the ADT molecule for DCM, CHF and DMAC. As seen in Figure 3.23, the ADT molecule exhibits the maximum peaks at 296, 297 and 295 nm, respectively. As can be seen from the relevant curves, the ADT molecule dissolved in DCM solution shows the largest and most stable spectrum. The ADT molecule is much more dominant in the near ultraviolet region.

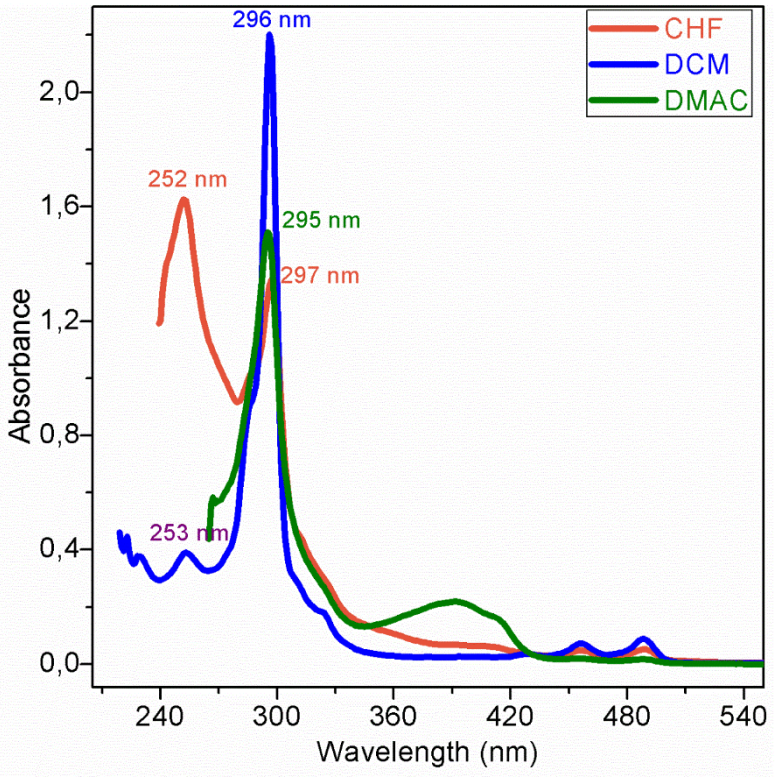

Figure 3.23. The absorbance spectra of the ADT molecule for DCM, CHF and DMAC solvents.

On the other hand, another important feature for studying the interaction of the material with light is reflectance (R). For this purpose, we also obtained reflectance measurements experimentally. The reflectance spectra of the ADT molecule for DCM, CHF and DMAC are shown in Figure 3.24. The ADT molecule exhibits much higher reflectance at lower wavelengths. At approximately 540 nm, the reflectance remains almost constant.

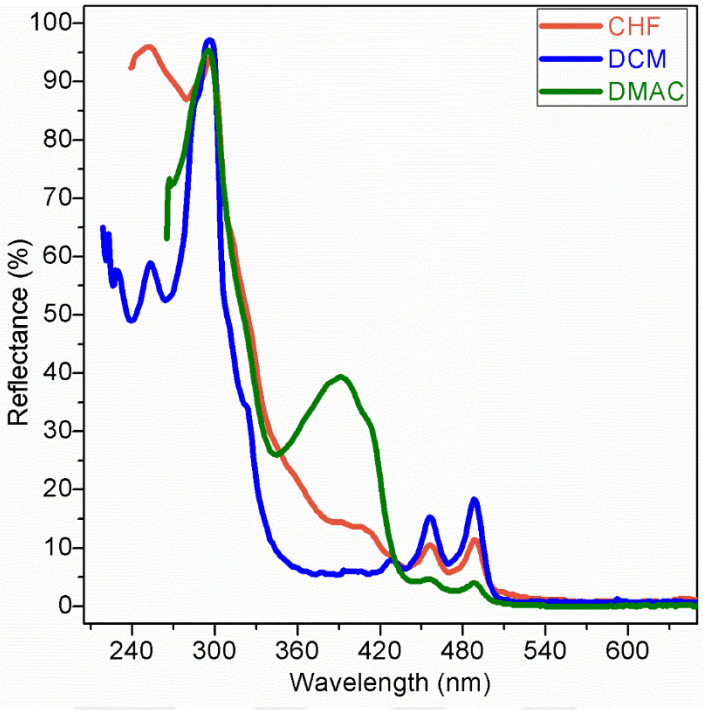

Figure 3.24. The reflectance spectra of the ADT molecule for DCM, CHF and DMAC solvents.

3.8. Experimental Optical Results for ADT Molecule

The optical band gap (E_g) is a significant optical parameter. The E_g of optical transitions of a material can be given by

$$\alpha(hv) = A^*\left(hv - E_g\right)^{1/2} \tag{3.2}$$

For ADT molecule, the best fitting was found to be for the plot of $(\alpha h\upsilon)^2$ versus photon energy (E) as seen in Fig. 3.25. That is, the type of the optical transition is the allowed direct transition and type of the optical band-gap is the allowed direct optical band gap (E_{gd}). We obtained allowed direct optical band gaps of the ADT molecule for DCM, CHF and DMAC solvents and found to be 2.452, 2.445 and 2.479 eV, respectively. According to these values, the lowest optical band gap was obtained for the CHF solvent, while the highest optical band gap was obtained for the DMAC solvent.

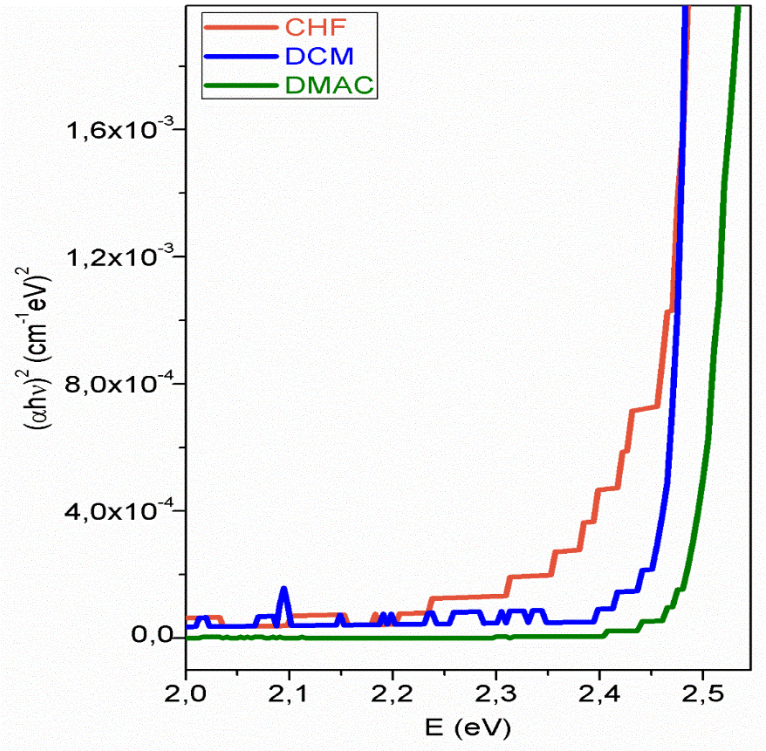

Figure 3.25. The plot of $(\alpha h\upsilon)^2$ versus photon energy (E) of the ADT molecule for DCM.

One of the most important optical parameters is the refractive index (n). The refractive index is obtained from the following equation,

$$n = \left\{ \left[\frac{4R}{(R-1)^2} - k^2 \right]^{1/2} - \frac{R+1}{R-1} \right\} \tag{3.3}$$

The refractive indices of the ADT molecule for DCM, CHF and DMAC solvents were obtained. Figure 3.26 shows the n curves of the ADT molecule. As shown in this Figure, the ADT molecule exhibits both normal and abnormal dispersion.

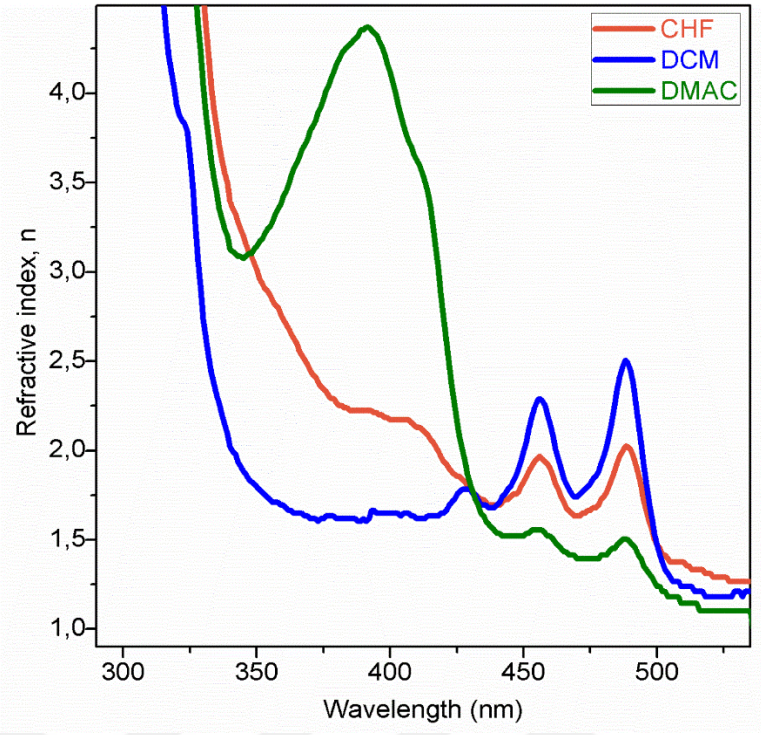

Figure 3.26. The refractive index (n) curves of the ADT molecule for DCM, CHF and DMAC solvents.

3.9. The Interpreting NMR Spectrum for ADT Molecule

NMR is significant since it provides a potent way to reckon the structure of organic molecules (OM). Organic chemists have utilized the NMR behavior of ^{1}H and ^{13}C nuclei because they provide precious data that can be utilized organic compound structure. The fundamental idea the NMR depend on outdoor magnetic field (MF). An MF creates due to move charge particle, then it will interact with an outdoor (MF), the two spin states have various energies, for instance, the spin state of +1/2 has a lower and -1/2 has higher in energy. The energy difference between two spin states grow due to increasing the MF, it means the energy difference is directly proportional to the intensity of the outdoor MF. When the sample absorbs the wavelength "energy" as the spins of nuclear are excited from +1/2 to -1/2, this is called resonance.

The ADT molecule has various net magnetic fields due to the different various amounts of electron density around various non-equivalent nuclei. At the MF strength the resonance frequency of ^{1}H nuclei are nearly 400 megahertz with a chemical shift approximately 10 ppm, the range of aromatic compound is observed between 6 ppm and 8.5 ppm. All of the figures are suitable with expectation value, for instance, as shown in Figure 3.27. But at the MF strength the resonance frequency of ^{13}C nuclei is nearly 100 megahertz with chemical shit around 200 ppm, the range of aromatic compound indicated between around 100 ppm and 150 ppm. As shown all of the diagrams below, in all of the figures are suitable with the expectation value.

Table 3.5 indicates the amount of chemical shit for ^{1}H that show in the NMR-spectrum for different basis sets. Also, Table 3.6. shows the amount of chemical shit for ^{13}C that show in the NMR spectrum for different basis sets.

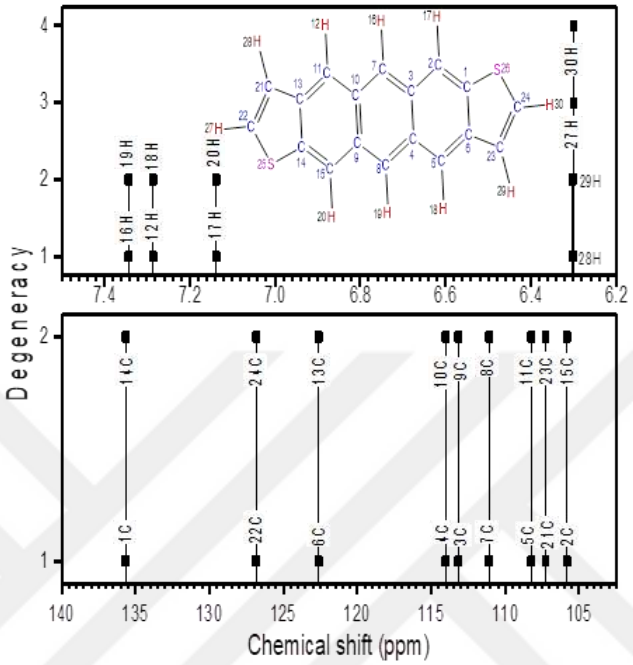

Figure 3.27. ^{1}H NMR and ^{13}C NMR spectra for ADT complex and for basis set 6-31G.

Figure 3.27 shows which H or C have more electronegativity and which of them have the same environment. There are 5 lines in the ^{1}H NMR spectrum, where there must be 10 lines for the hydrogen atom in the ADT compound. This indicates that two of each hydrogen have the same environment. Also, for carbons, there must be 18 lines, but there are 9 lines. The electronegative in 16H and 19H is more comparing with another one, the environment for 16H and 19H have the same. Also, 1C and 14C have more electronegativity comparing with another one.

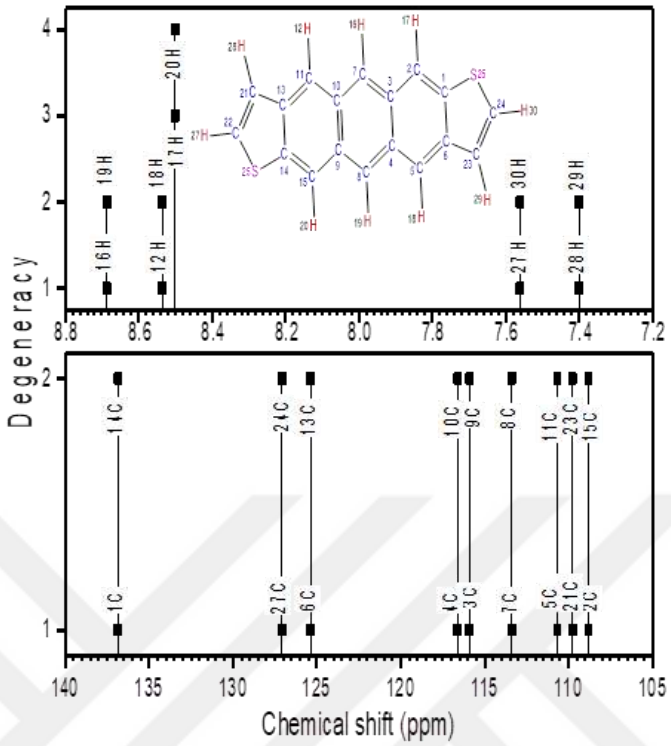

Figure 3.28. ^{1}H NMR and ^{13}C NMR spectra for ADT complex and for basis set 6-31G (d, p).

Figure 3.28 shows the five lines in a different place in the 1H spectrum and the nine lines in a different place in the ^{13}C spectrum. It means that they have a different environment due to different electronegativity. The peak at about 8.7 of the large chemical shifts is due to 16H and 19H since they have more electronegative atom attached. Also, 1C and 14C have more electronegativity comparing with 2C and 15C.

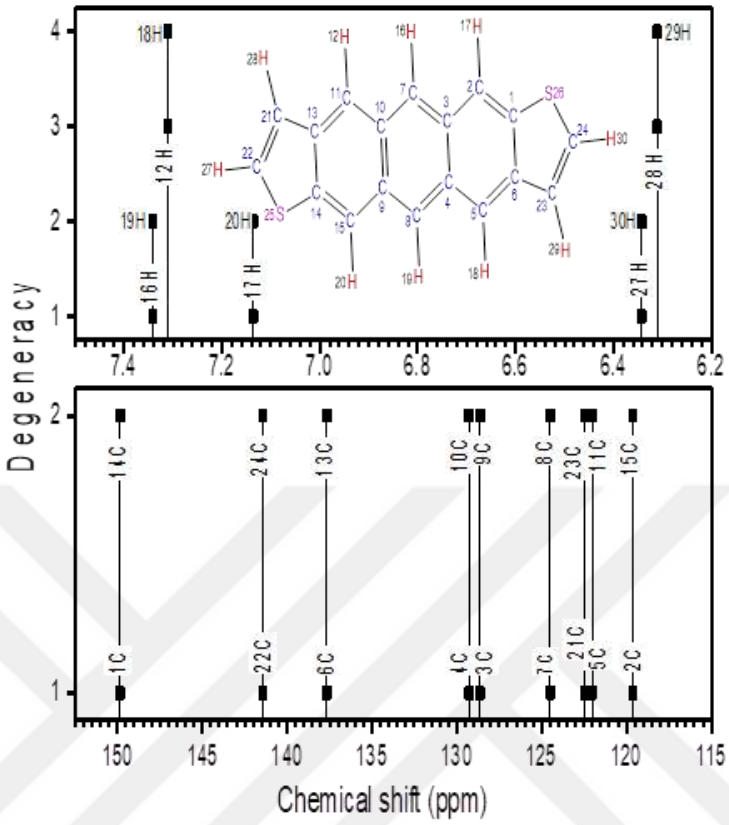

Figure 3.29. ^{1}H NMR and ^{13}C NMR spectra for ADT complex and for basis set 6-311G.

Figure 3.29 indicates that 16H and 19H have more electronegativity, it means more electron density around them, comparing with 28H and 29H. The range in ^{1}H NMR spectrum, chemical shift is nearly around from 6.33 ppm to 7.33 ppm. Also, 1C and 14C have more electronegativity comparing with the 2C and 15C. The range in ^{13}C NMR spectrum, chemical shift is nearly around from120 ppm to 150 ppm.

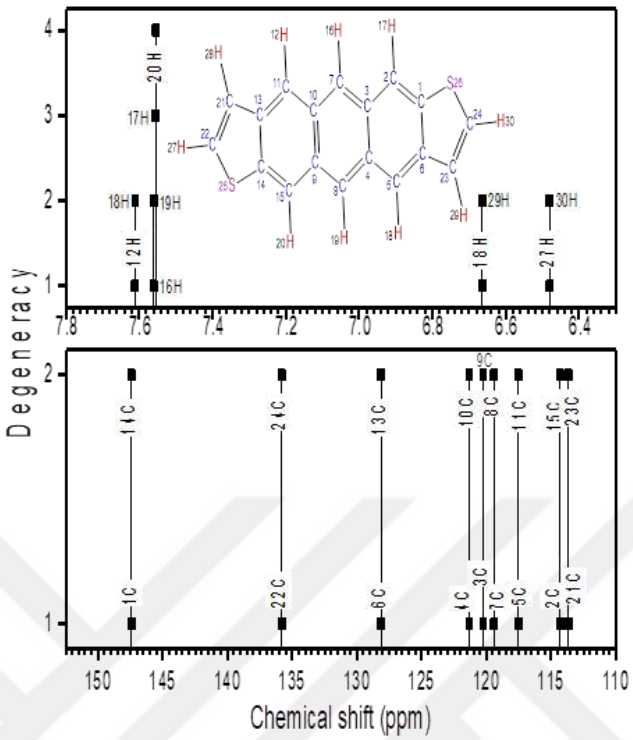

Figure 3.30. ^{1}H NMR and ^{13}C NMR spectra for ADT complex and for basis set LanL2DZ.

Figure 3.30 shows that the 7H and 30H have less electronegativity, whenever the 28H and 29H have less electronegativity by using the basis sets {6-31G (d, p) and 6-311G}. Also, the 21C and 23C have less electronegativity, while, the 2C and 15C have less electronegativity by using the basis sets {6-31G, 6-31G (d, p) and 6-311G}.

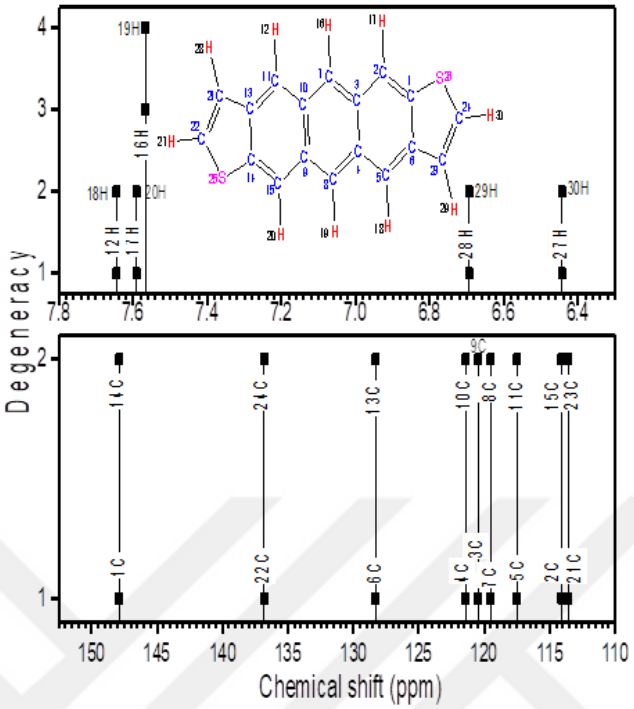

Figure3.31. 1H NMR and 13C NMR spectra for ADT complex and for basis set DSS.

Figure 3.31 illustrates the shielding from the outdoor magnetic field and the electronegativity on the hydrogen H and carbon C to know which H have more electronegativity and which carbon have more electronegativity, they will absorb electromagnetic radiation of low energy. The 12H and 18H have the same environment and they have more electronegativity. The 1C and 14C have the same environment and they have more electronegativity.

Table 3.4. [1]H NMR chemical shifts of the ADT molecule.

	Chemical shift (ppm)						
Assignment	6-31G	6-31G(d, p)	6-311G	LanL2DZ	DSS	Average	Degeneracy
28H	6.30	7.40	6.31	6.66	6.69	6.67	1,3
29H	6.30	7.40	6.31	6.66	6.69	6.67	2,4
27H	6.29	7.56	6.34	6.48	6.44	6.62	3,1
30H	6.29	7.56	6.34	6.48	6.44	6.62	4,2
17H	7.13	8.50	7.13	7.55	7.59	7.58	1,3
20H	7.13	8.50	7.13	7.55	7.59	7.58	2,4
12H	7.28	8.53	7.31	7.61	7.64	7.67	1,3
18H	7.28	8.53	7.31	7.61	7.64	7.67	2,4

Table 3.5. (Continue)

16H	7.34	8.68	7.34	7.55	7.56	7.69	1,3
19H	7.34	8.68	7.34	7.55	7.56	7.69	2,4

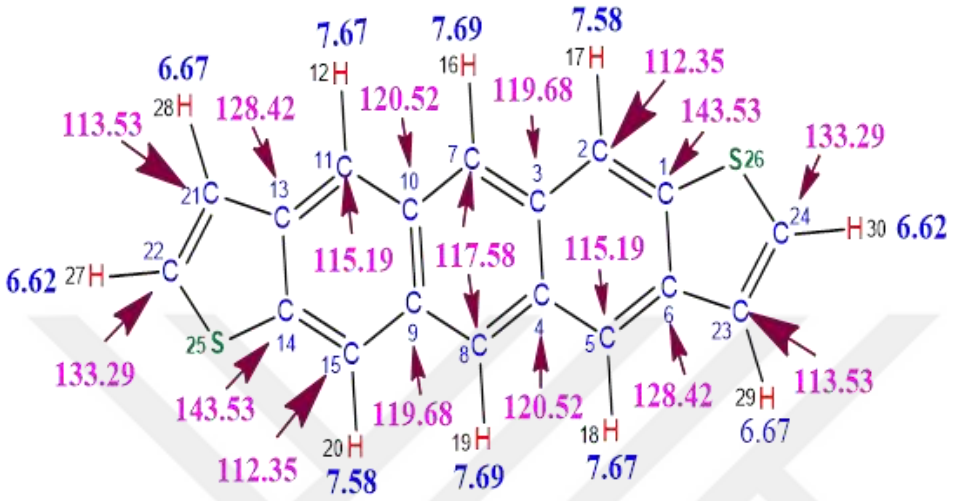

Figure 3.32. Indicate average chemical shifts (ppm) by using the DFT with five basis sets.

Table 3.6. ^{13}C NMR chemical shifts of the ADT molecule.

	Chemical shift (ppm)						
Elements	6-31G	6-31G(d, p)	6-311G	LanL2DZ	DSS	Average	Degeneracy
2C	105.83	108.81	119.62	114.29	114.09	112.35	1
15C	105.83	108.81	119.62	114.29	114.09	112.53	2
21C	107.27	109.77	122.48	113.65	113.56	113.53	1
23C	107.27	109.77	122.48	113.65	113.56	113.53	2
5C	108.23	110.67	122.02	117.53	117.50	115.19	1
11C	108.23	110.67	122.02	117.53	117.50	115.19	2
7C	111.10	113.39	124.49	119.39	119.51	117.58	1
8C	111.10	113.39	124.49	119.39	119.51	117.58	2
3C	113.16	115.90	128.64	120.24	120.47	119.68	1
9C	113.16	115.90	128.64	120.24	120.47	119.68	2
4C	114.02	116.60	129.27	121.32	121.41	120.52	1
10C	114.02	116.60	129.27	121.32	121.41	120.52	2
6C	122.62	125.38	137.67	128.14	128.31	128.42	1
13C	122.62	125.38	137.67	128.14	128.31	128.42	2
22C	126.85	127.08	141.44	135.80	136.80	133.29	1
24C	126.85	127.08	141.44	135.80	136.80	133.29	2
1C	135.66	136.84	149.85	147.41	147.90	143.53	1
14C	135.66	136.84	149.85	147.41	147.90	143.53	2

The table gives information about the chemical shift by using the DFT with some basis sets. It is noticeable that chemical shift increases from the top to the bottom of this table

4. CONCLUSIONS

In conclusion, the DFT techniques along with B3LYP, with some basis sets were utilized for optimizing the Anthradithiophene (ADT). After optimization, it was shown the electrostatic potential map (EPM), it indicated that the sulfurs have greatest electronegativity value and the hydrogens have the smallest electronegativity value.

In this work, first, HOMO and LUMO have utilized for computation the bad-gap energy. The average band-gap energy between the HOMO and LUMO was found to be 2.84 eV by using five basis sets. After that, the FTIR has been elucidated, in addition, to determine the functional group and determined the important region that did not take place absorption, in general, this region that did not occur absorption is around between the 1650 cm-1 and 3200 cm-1, by suing five basis sets. Then, the UV-Vis spectroscopy was elucidated, in addition, to determine the energy band-gap, that the average energy band gap was found to be 2.59 eV, and it was determined the correct transition type, the ADT molecule exhibited the direct allowed transition.

Finally, NMR spectroscopy was elucidated for determining the which hydrogen and carbon have more shielded. Obtained results shows that the 16H and 19H have the same environment and they have less shielded comparing with another hydrogen, as well as, the carbon 1C and 14C have the same environment and they have less shielded comparing with another carbon. The NMR spectra indicated that each of the (16H and 19H), (12H and 18H), (17H and 20H), (28H and 29H) and (27H and 30H) have the same environment, it means they have the same electronegativity. As well, for each of the (1C and 14C), (22C and 24C), (6C and 13C), (4C and 10C), (3C and 9C), (7C and 8C), (5C and 11C), (21C and 23C) and (2C and 15C) have the same environment or around them have them have the same electron density. In addition, the experimental result and theoretical are suitable.

REFERENCES

[1] Gross, E., Runge, E., and Heinonen, O., Many-Particle Theory (Adam Hilger,) (1991), AbeBooks Press, Munich, Germany.

[2] Szabo, A. and Ostlund, N.S., (2012). Modern quantum chemistry: introduction to advanced electronic structure theory, Dover Publications, Mineola, New York, USA.

[3] Griffiths, D.J. and Schroeter, D.F., (2018). Introduction to quantum mechanics, Cambridge University Press, Cambridge, UK.

[4] Campbell, I., Kress, J., Martin, R., Smith, D., Barashkov, N., and Ferraris, J., (1997). Controlling charge injection in organic electronic devices using self-assembled monolayers, Applied physics letters, 71(24), 3528-3530.

[5] Kohn, W., (1999). Nobel Lecture: Electronic structure of matter—wave functions and density functionals, Reviews of Modern Physics, 71(5), 1253.

[6] Hohenberg, P. and Kohn, W., (1964). Inhomogeneous electron gas, Physical review, 136(3B), 864.

[7] Tu, G., (2008). Studies of self-interaction corrections in density functional theory, Universitetsservice, US-AB, Sweden.

[8] Reine, S.S., (2009). Density functional theory for large molecular systems, in The Journal of Chemical Physics 133(4):044102.

[9] Vanhoof, V., (2006). Density functional theory studies for transition metals: small (Fe, Co)-clusters in fcc Ag, and the spin density wave in bcc Chromium, Instituut voor Kern- en Stralingsfysica, K.U.Leuven, Belgium.

[10] Abreu, J., (2015). Density Functional Theory: Systematic benchmarking of exchange and correlation functionals for the G2 dataset, Master of Science, University of Coimbra, Portugal.

[11] Kohn, W. and Sham, L.J., (1965). Self-consistent equations including exchange and correlation effects, Physical review, 140(4A), A1133.

[12] Samal, P., (2006). Studies In Excited-State Density-Functional Theory, Indian Institute Of Technology Kanpur India.

[13] Abrahão, C.A., Bomfim, E., Lopes-Júnior, L.C., and Pereira-da-Silva, G., (2019). Complementary Therapies as a Strategy to Reduce Stress and Stimulate Immunity of Women With Breast Cancer, Journal of evidence-based integrative medicine, 24, 2515690X19834169.

[14] Cottenier, S., (2002). Density Functional Theory and the family of (L) APW-methods: a step-by-step introduction, Instituut voor Kern-en Stralingsfysica, KU Leuven, Belgium, 4(0), 41.

[15] Zwettler, N., Density functional theory, Institute for Physics, Theoretical Physics, University of Graz, Austria.

[16] Chang, R., (2005). Physical chemistry for the biosciences, University Science Books, University Science Books, Sausalito, California, USA.

[17] Capelle, K., (2006). A bird's-eye view of density-functional theory, Brazilian Journal of Physics, 36(4A), 1318-1343.

[18] Tsuneda, T., (2014). Density functional theory in quantum chemistry, Springer, Japan.

[19] Sena, A.M.P., (2010). Density functional theory studies of surface interactions and electron transfer in porphyrins and other molecules, University College London, UK.

[20] Lewars, E., (2003). Introduction to the theory and applications of molecular and quantum mechanics, J. Computational chemistry, Ontario Canada.

[21] Onishi, T., (2018). Quantum Computational Chemistry, Modelling and Calculation for Functional Materials, Springer Nature, Singapore.

[22] Young, D., (2004). Computational chemistry: a practical guide for applying techniques to real world problems, John Wiley Press, USA.

[23] Hehre, W.J., (2003). A guide to molecular mechanics and quantum chemical calculations, Wavefunction, Inc., Irvine, California, USA.

[24] Mueller, M.P., (2007). Fundamentals of quantum chemistry: molecular spectroscopy and modern electronic structure computations, Springer Science & Business Media, USA.

[25] Helgaker, T., Jorgensen, P., and Olsen, J., (2014). Molecular electronic-structure theory, John Wiley Press. USA.

[26] Piela, L., (2006). Ideas of quantum chemistry, Elsevier Science, University of Warsaw, Warsaw, Poland.

[27] Jensen, F., (2017). Introduction to computational chemistry, John Wiley Press, USA.

[28] Atkins, P.W. and Friedman, R.S., (2011). Molecular quantum mechanics, Oxford University Press, Oxford, England.

[29] Bachrach, S.M., (2014). Computational organic chemistry, John Wiley Press, USA.

[30] Becke, A.D., (1988). Density-functional exchange-energy approximation with correct asymptotic behavior, Physical Review A, 38(6), 3098.

[31] Stephens, P., Devlin, F., Chabalowski, C., and Frisch, M.J., (1994). Ab initio calculation of vibrational absorption and circular dichroism spectra using density functional force fields, The Journal of Physical Chemistry, 98(45), 11623-11627.

[32] Krieger, J., Li, Y., and Iafrate, G., (1992). Construction and application of an accurate local spin-polarized Kohn-Sham potential with integer discontinuity: Exchange-only theory, Physical Review A, 45(1), 101.

[33] McHale, J.L., (2017). Molecular spectroscopy, Taylor & Francis Group, New York, USA.

[34] Perkampus, H.-H., (2013). UV-VIS Spectroscopy and its Applications, Springer-Verlag Berlin Heidelberg, Germany.

[35] Larkin, P., (2017). Infrared and Raman spectroscopy: principles and spectral interpretation, Elsevier. Stamford, Connecticut, USA.

[36] Freeman, R., (2003). Magnetic resonance in chemistry and medicine, Oxford University Press, Oxford, England.

[37] Lambert, J.B., Mazzola, E.P., and Ridge, C.D., (2019). Nuclear magnetic resonance spectroscopy: an introduction to principles, applications, and experimental methods, John Wiley Press, USA.

[38] Morris, G., (1987). Atta-Ur-Rahman. Nuclear magnetic resonance: Basic principles. Springer-Verlag, Berlin, Heidelberg, New York, Tokyo, 1986. 358 pp. DM128. ISBN 3 540 96243 3, Magnetic Resonance in Chemistry, 25(4), 375-375.

[39] Akitt, J.W. and Mann, B.E., (2017). NMR and Chemistry: An introduction to modern NMR spectroscopy, Taylor & Francis Group, New York, USA.

[40] Kwon, O., Coropceanu, V., Gruhn, N., Durivage, J., Laquindanum, J., Katz, H., Cornil, J., and Brédas, J.-L., (2004). Characterization of the molecular parameters determining charge transport in anthradithiophene, The Journal of chemical physics, 120(17), 8186-8194.

[41] Brédas, J.-L., Calbert, J.P., da Silva Filho, D., and Cornil, J., (2002). Organic semiconductors: A theoretical characterization of the basic parameters governing charge transport, Proceedings of the National Academy of Sciences, 99(9), 5804-5809.

[42] Miao, Q., (2015). Polycyclic Arenes and Heteroarenes: Synthesis, Properties, and Applications, John Wiley Press, USA.

[43] Wang, W.-C., Yeh, T.-T., Liau, W.-L., Chen, J.-T., and Hsu, C.-S., (2018). Anthradithiophene-based liquid crystal molecules: High carrier mobilities enhanced by rubbed polyimides for the application in organic field-effect transistors, Organic Electronics, 57, 82-88.

[44] Conrad, B.R., Chan, C.K., Loth, M.A., Anthony, J.E., and Gundlach, D.J. (2009). Electrical characterization of soluble anthradithiophene derivatives. in International Semiconductor Device Research Symposium, John Wiley Press, USA.

[45] Balandier, J.-Y., Quist, F., Sebaihi, N., Niebel, C., Tylleman, B., Boudard, P., Bouzakraoui, S., Lemaur, V., Cornil, J., and Lazzaroni, R., (2011). Donor/acceptor-substituted anthradithiophene materials: synthesis, optical and electrochemical properties, Tetrahedron, 67(37), 7156-7161.

[46] Liu, Q., Liu, Y., Wang, Y., Ai, L., Ouyang, X., Han, L., and Ge, Z., (2013). Anthradithiophene-benzothiadiazole-based small molecule donors for organic solar cells, New Journal of Chemistry, 37(11), 3627-3633.

[47] Jurchescu, O.D., Subramanian, S., Kline, R.J., Hudson, S.D., Anthony, J.E., Jackson, T.N., and Gundlach, D.J., (2008). Organic single-crystal field-effect transistors of a soluble anthradithiophene, Chemistry of Materials, 20(21), 6733-6737.

[48] Li, S., Ryno, S.M., and Risko, C., (2018). Exploring thermal transitions in anthradithiophene-based organic semiconductors to reveal structure-packing relationships, Journal of Materials Chemistry C, 6(40), 10924-10934.

[49] Day, J., (2008). On the photoresponse of several novel functionalized oligoacene and anthradithiophene derivatives, Oregon State University, Corvallis, USA.

[50] Bao, Z. and Locklin, J., (2007). Organic field-effect transistors, Taylor & Francis Group, New York, USA.

[51] Nasrallah, I., Banger, K.K., Vaynzof, Y., Payne, M.M., Too, P., Jongman, J., Anthony, J.E., and Sirringhaus, H., (2014). Effect of Ozone on the Stability of Solution-Processed Anthradithiophene-Based Organic Field-Effect Transistors, Chemistry of Materials, 26(13), 3914-3919.

[52] Platt, A.D., Day, J., Subramanian, S., Anthony, J.E., and Ostroverkhova, O., (2009). Optical, fluorescent, and (photo) conductive properties of high-performance functionalized pentacene and anthradithiophene derivatives, The Journal of Physical Chemistry C, 113(31), 14006-14014.

[53] Liu, Q.D., Peng, R.X., Chen, S.J., Ai, L., Wang, S.Y., Liu, Z.Y., and Ge, Z.Y., (2014). Synthesis and Photovoltaic Properties of New Multifused Anthradithiophene-Based Narrow-Bandgap D–A Copolymers, Macromolecular Chemistry and Physics, 215(13), 1287-1296.

[54] Schön, J., Kloc, C., Siegrist, T., Laquindanum, J., and Katz, H., (2001). Charge transport in anthradithiophene single crystals, Organic Electronics, 2(3-4), 165-169.

[55] Hallani, R.K., Thorley, K.J., Mei, Y., Parkin, S.R., Jurchescu, O.D., and Anthony, J.E., (2016). Structural and electronic properties of crystalline, isomerically pure anthradithiophene derivatives, Advanced functional materials, 26(14), 2341-2348.

[56] Laquindanum, J.G., Katz, H.E., and Lovinger, A.J., (1998). Synthesis, morphology, and field-effect mobility of anthradithiophenes, Journal of the American Chemical Society, 120(4), 664-672.

[57] Mamada, M., Katagiri, H., Mizukami, M., Honda, K., Minamiki, T., Teraoka, R., Uemura, T., and Tokito, S., (2013). Syn-/anti-anthradithiophene derivative isomer effects on semiconducting properties, ACS applied materials & interfaces, 5(19), 9670-9677.

[58] Hallani, R.K., (2015). Designing anthradithiophene derivatives suitable for applications in organic electronics and optoelectronics, UKnowledge, University of Kentucky, Lexington, Kentucky, USA.

CURRICULUM VITAE

Hazhar HAMAD RASUL

PERSONAL INFORMATIONS

Birth of Place	**:** Erbil-Iraq
Birth of Date	**:** 27.10.1991
Nationalty	**:** Iraq
Address	**:** Salahaddin University-Erbil
E-mail	**:** hazharhrm@gmail.com
Languages	**:** English (A1)

EDUCATION

Bachelor	**:** Salahaddin University-Erbil, College of Science
High School	**:** Chwar-Qwrna Coeducation Preparatory

RESEARCH EXPERIENCES

- ✓ GaussView Software and Origin Lab Software